Publication Year	2015
Acceptance in OA @INAF	2020-04-20T10:31:35Z
Title	LOFT as a discovery machine for jetted Tidal Disruption Events
Authors	Rossi, E. M.; Donnarumma, I.; Fender, R.; Jonker, P.; Komossa, S.; et al.
Handle	http://hdl.handle.net/20.500.12386/24106

Italian Science Case for ALMA Band 2+3[*]

M. T. Beltrán[1], E. Bianchi[1], J. Brand[2], V. Casasola[1], R. Cesaroni[1], C. Codella[1], F. Fontani[1], L. Gregorini[3], G. Guidi[1], L. Hunt[1], E. Liuzzo[2], A. Marconi[4], M. Massardi[2], L. Moscadelli[1], R. Paladino[2], L. Podio[1], I. Prandoni[2], V. Rivilla[1], K. L. J. Rygl[2], L. Testi[1,5]

1 Introduction

The Premiale Project "Science and Technology in Italy for the upgraded ALMA Observatory – iALMA" has the goal of strengthening the scientific, technological and industrial Italian contribution to the Atacama Large Millimeter/submillimeter Array (ALMA), the largest ground based international infrastructure for the study of the Universe in the microwave. One of the main objectives of the Science Working Group (SWG) inside iALMA, the Work Package 1, is to develop the Italian contribution to the Science Case for the ALMA Band 2 or Band 2+3 receiver. ALMA Band 2 reveiver spans from ~ 67 GHz (bounded by an opaque line complex of ozone lines) up to 90 GHz which overlaps with the lower frequency end of ALMA Band 3. Receiver technology has advanced since the original definition of the ALMA frequency bands. It is now feasible to produce a single receiver which could cover the whole frequency range from 67 GHz to 116 GHz, encompassing Band 2 and Band 3 in a single receiver cartridge, a so called Band 2+3 system. In addition, upgrades of the ALMA system are now foreseen that should double the bandwidth to 16 GHz. The science drivers discussed below therefore also discuss the advantages of these two enhancements over the originally foreseen Band 2 system.

2 Galactic Science

2.1 High-mass star formation

High-mass stars are commonly defined as those stars whose mass exceeds ~ 8 $M_\odot$, a limit that may vary depending on the border conditions, such as, e.g., the accretion rate. What makes these stars different from their low-mass siblings, is that they reach the zero-age main sequence still undergoing heavy accretion. While the theoretical details of the high-mass star formation process are still a matter of debate, a solid observational finding is that young OB-type stars are deeply embedded inside their parental molecular cores – the so-called hot molecular cores (HMCs). At the same time, massive stars are known to form in rich stellar clusters and are located at typical distances of a few kpc. All these facts make it very difficult to study the cirumstellar environment, due to the large extinction and small separation from the nearby cluster members. These constraints call for high angular resolution ($\ll 1''$) observations at long

---

[1]INAF-Osservatorio Astrofisico di Arcetri, Largo E. Fermi 5, 50125, Firenze, Italy
[2]INAF-Istituto di Radioastronomia, via Gobetti 101, 40129 Bologna, Italy
[3]Dipartimento di Fisica e Astronomia, Università di Bologna, Viale Berti Pichat 6/2, 40127 Bologna, Italy
[4]Dipartimento di Fisica e Astronomia, Università di Firenze, Largo E. Fermi 2, I-50125 Firenze, Italy
[5]ESO, Karl-Schwarzschild-Strasse 2, 85748 Garching bei München, Germany

wavelengths, where the dust opacity is sufficiently low. In practice, interferometric observations at (sub)mm wavelengths are the ideal tool to investigate these regions.

Another important characteristic of young massive stars is that they are surrounded by dense gas, rich in molecular species. These are believed to form on grains and then be released to the gas phase when the grain mantles are evaporated by the photons of the newly born star. As a matter of fact, the rotational transitions of rare, complex species can be effectively used to derive the physical parameters of the circumstellar gas and study its distribution and velocity field. Moreover, detailed census of many molecular species may allow one to derive the chemical composition of the gas and thus decide what reactions may explain the formation of the observed molecules, which in turn may shed light on the genesis of the star itself.

With all this in mind, there is little doubt that ALMA is the ideal instrument for studies of high-mass star formation. The unprecedented angular resolution in the (sub)mm regime coupled with the high sensitivity, as well as the broad, simultaneous frequency coverage, are bound to satisfy all the requirements discussed above. In particular, the dust opacity in molecular clouds is known to increase with frequency, which makes it convenient to observe at (sufficiently) long wavelengths. However, one must also keep in mind that all rotational transitions of molecules lie in the (sub)mm range, which sets a lower limit to λ. Therefore, as a rule of thumb, observations of high-mass star forming regions are best performed between a few mm and a few 100 μm.

In the following, we identify three major contributions that ALMA Band 2+3 may give to the study of high-mass star formation.

2.1.1 The chemical content of HMCs

As discussed in more detail in other parts of this report, the study of the chemical content of HMCs is expected to help us to set tight constraints on the star formation process. But what is the best frequency range for this type of studies? To answer this question, it is important to stress that the number of rotational transitions is increasing with decreasing wavelength and their excitation energies are on average higher. If the "quantity" of the information obtained from broad band observations increases dramatically with the observing frequency, the corresponding "quality" is not necessarily improving. In fact, one sees that the overwhelming number of lines detected towards HMCs often hinders precise line identifications due to multiple overlaps of adjacent transitions. Moreover, the high excitation energies make such lines weaker and their emitting regions significantly smaller than those traced by lower excitation (and lower frequency) transitions. These problems make it very difficult and sometimes even impossible to resolve both in space and velocity the emission from different species. For HMC studies it may thus be worthy to perform observations at longer wavelengths. In this context the ALMA Band 2+3 project will play a crucial role.

Another aspect that also favours the choice of low frequencies for studies of HMC chemistry, is the dust opacity. The dust optical depth in the (sub)mm domain increases with frequency as $\tau \propto N_{\mathrm{H_2}} \nu^\beta$, where $\beta \simeq 1$–2 and $N_{\mathrm{H_2}}$ is the $\mathrm{H_2}$ column density along the line of sight through the HMC. Clearly, this implies that at sufficiently large frequencies the core will become optically thick and the line photons will be absorbed by the dust, thus reducing the observed line intensities dramatically. This effect is bound to affect especially the transitions of the typical HMC tracers, as opposed to those molecules that are present (also) in the surrounding, lower density envelope. For the same reason, the effect will be more prominent in the innermost parts of the HMCs, because the density is believed to increase towards the core center as a power law, which boosts the value of the dust opacity. While it is difficult to establish the frequency and radius at which the dust opacity will overcome the line emission, it seems likely that in the ALMA Band 2+3 such an effect will be negligible: in fact even for a column density as high as $N_{\mathrm{H_2}} = 10^{25}$ cm^{-2}, the dust opacity at, e.g., 85 GHz is only $\tau \simeq 0.01 \ll 1$.

2.1.2 Infall studies

One of the important issues concerning the formation of an OB-type star is the time at which accretion stops. Some authors (see Keto 2002) have proposed that accretion onto the star may initially quench the formation of an HII region, until the stellar mass has increased to the point that the Lyman continuum luminosity overcomes the mass accretion rate. This model predicts also that even after the formation of an ionized region around the star, acrretion should go on through the HII region itself. It is thus interesting to establish observationally whether infall can be detected towards the youngest HII regions. In particular, hypercompact HII regions (see Kurtz 2005) should be the ideal targets to detect red-shifted absorption in suitable molecular lines.

To search for red-shifted absorption towards these objects, one needs a good tracer of the infalling gas and a bright HII region. Unfortunately, these two requirements are to some extent conflictual, as the brightness temperature of the free-free emission decreases with frequency, wehereas the number of molecular lines increases (as explained above). It is thus necessary to find a compromise and select the longest possible wavelength where a sufficient number of rotational transitions can be found. Cesaroni (2008) demonstrates that employing observations at frequencies below $\sim$100 GHz even infall towards hypercompact HII regions around stars as late as B3 can be detected.

One should keep in mind that infall studies with molecular lines may be nicely complemented by observations of recombination lines, which trace the ionized gas of the HII region. Given the broad ALMA frequency coverage, it will be possible to perform observations of both suitable molecular lines to detect infall *towards* the HII region, and a recombination line to trace the infall *inside* the HII region.

2.1.3 Circumstellar disks

It is known that circumstellar accretion disks around B- and even more O-type stars appear to be elusive (see Cesaroni et al. 2007 for a review). Recently, the existence of such disks around B-type stars has found further support from observations with ALMA (see Sánchez-Monge et al. 2013, 2014; Beltrán et al. 2014) and similar results are expected also for O-type stars when the longest array baselines will be available. Clearly, angular resolution is an important issue in this type of studies, which calls for high-frequency observations. However, one should not forget that also low-frequency lines may be worthy. As previously explained, most high-frequency transitions arise from high-energy levels and hence trace the innermost regions of the disk. Therefore, the advantage of a better angular resolution is basically compensated by the smaller emitting region. One may roughly conclude that the ratio between source angular size and instrumental beam is approximately independent of the observing frequency.

Despite this consideration, the study of disks around O-type stars is likely best performed at high frequencies, given the expected size of the disks (a few 1000 au) and the large distances of the objects (several kpc), but observations at ALMA Band 2+3 may play an important role to investigate the structure of the nearest (2–3 kpc) disks around B-type stars. Beside the advantages already discussed above (limited line overlap, negligible dust absorption), observations at low frequencies are less affected by phase instabilities and allow to target objects at lower elevations. The linear resolution achievable at 3 mm ($\sim$50 mas) will suffice to resolve the disk plane and establish for example the presence of spiral arms. The targets for this type of observations will be known luminous ($\sim$$10^4$ $L_\odot$) (proto)stars for which evidence of circumstellar disks has been previously found with Plateau de Bure and ALMA observations.

2.2 High-mass star-formation under the magnifying glass

2.2.1 High-mass star forming regions with methanol masers

As already mentioned, some of the biggest challenges in high-mass star formation (HMSF) studies is the identification of high-mass star-forming objects and understanding how mass accretion continues beyond a stellar mass of $8\,M_\odot$ (Palla & Stahler 1993). With the advance of mm-interferometry, many massive cores have been found to fragment to lower mass proto-stellar objects, and multiplicity in star formation is often difficult to exclude, casting doubts on masses of single star-forming objects. The search for accretion discs, predicted by recent 2-D models of HMSF (e.g., Kuiper et al. 2010) and considered essential for continuing accretion despite the stellar radiation pressure, is only possible through high angular resolution kinematic studies of the gas surrounding the protostar, searching for disc signatures and/or jets emitted along the disc axis.

The methanol maser emission at 6.7 GHz is one of the strongest and most widespread interstellar masers (Menten et al. 1991). It can be used both for pinpointing high-mass star-forming regions (HMSFRs) and for determining the structure and kinematics of the gas at high resolution. As the excitation of this maser transition requires high densities and strong infrared emission and/or shocks (Sobolev & Deguchi 1994, Cragg et al 2005), methanol masers are found exclusively toward HMSFRs (Minier et al. 2003). Their brightness and compactness make the methanol masers an excellent tool for astrometry (Rygl et al. 2010) and structure and 3-D velocity studies at distances of 10–1000 AU from the newly born high-mass star (e.g., Moscadelli et al. 2011). VLBI imaging of 6.7 GHz methanol masers showed that in ~30% of the sources they are distributed in a ring-like shape (with radii of 20–200 mas) around the central protostar, with kinematics suggesting that these masers originate at the interface between the protostellar outflow and a disc or torus (Bartkiewicz et al. 2009). Though the 6.7 GHz masers environments have been identified only in a few high-mass protostars (e.g., Sanna et al. 2010, 2014, Moscadelli et al. 2011), the 6.7 GHz maser emission was found to trace both disc rotation and expansion, the latter likely induced by interaction with protostellar wind/jet, suggesting that ring-shaped methanol masers are the ideal high-mass disc-candidates.

2.2.2 Justification for ALMA Band 2+3

Ring-like methanol maser sources in continuum emission with ALMA   A high-angular resolution continuum and molecular line study with ALMA in Band 2+3 of the ring-shaped 6.7 GHz methanol masers could find conclusive evidence of discs, outflows, and constrain the evolutionary stage of the high-mass protostar. Two emission mechanisms can contribute to the spectral energy distribution of disc candidates: free-free emission from the ionized gas and thermal black body emission from the dusty envelope. In its turn, the free-free emission associated with these maser sources can originate both from hyper- or ultra-compact HII regions and ionized, wide-angle or collimated, stellar winds. Following the paradigm of the disc/jet system, one would expect to observe a flaring dusty envelope, oriented perpendicular to the ionized jet.

Establishing the nature and structure of the protostellar continuum requires sensitive (rms noise $\lesssim 10\,\mu$Jy), high angular resolution ($\theta_{\rm FWHM} < 100$ mas) imaging in the mm wavelength range. The ALMA Band 2+3 frequency range, from 67 to 116 GHz, is crucial to visualize the distribution of the continuum emission and separate the free-free emission from the thermal dust component by means of the spectral index, α, analysis. In fact, while the free-free emission is expected to be optically thin ($\alpha \sim 0$) in this frequency range, the dust emission should rapidly increase with frequency ($\alpha > 1$). Previous observations show that above a detection threshold of a few $100\,\mu$Jy only a small fraction of ring shaped methanol masers (10%) is associated with cm continuum emission, which motivated the interpretation that these sources harbor young

Hɪɪ regions with a high turnover frequency (Bartkiewicz et al. 2009). ALMA will achieve an extraordinary sensitivity at 3-5 mm, rms noise $<10\,\mu$Jy in less than one hour, allowing one to image much weaker free-free emission than in previous cm studies, and possibly finding dusty flattened disc structures (Sanna et al. 2014). ALMA's long baseline configuration of ~ 15 km offers $\sim$ 70 and 40 mas resolution at 5 and 3 mm, respectively, sufficient to resolve structures that have similar angular scales as the observed maser rings.

Ring-like methanol maser sources in spectral line emission with ALMA Simultaneously with the continuum observations, ALMA can perform high-resolution imaging of the disc/jet structure in various molecular lines available in Band 2+3, such as the low-J HCO$^+$ and SiO transitions, and various deuterated species (see other contributions in this white paper) that can be compared to the structure of the maser ring. If the envelope is truly flattened, then one might observe an inner gap at radii smaller than the methanol maser ring, since temperature and turbulence should be too high for these molecular species to survive.

In summary, ALMA Band 2+3 observations of ring shaped methanol masers, will offer a wealth of continuum and molecular data that could provide crucial evidence for disc structures around high-mass star-forming objects.

2.3   Low excitation lines of deuterated molecules

There are no doubts that the two most important chemical processes occuring in the cold (T $\leq$ 20 K) and dense ($\geq 10^4$ cm^{-3}) pre–stellar cores are: *(i)* the enhancement of deuterated molecules, and *(ii)* the freeze-out of neutral atoms and molecules on the surface of dust grains, where the depletion of both C-bearing and N-bearing molecules is found to be high in low- and high-mass pre–stellar cores. The first one, initiated mainly from the proton-deuteron exchange reaction $H_3^+ + HD \rightarrow H_2D^+ + H_2 + \Delta E$, is favoured at low temperature because of the endothermicity of the backward chemical reaction. The second one, occurring on the surfaces of dust grains, is favoured by the combination of low temperature and high density, by which atoms and molecules stick on the surface of a dust grain and remain frozen on it (see Caselli & Ceccarelli for a review). The two processes are believed to be correlated in the cold gas: in fact, depletion of CO boosts the deuterium fractionation process because other neutrals can combine with the abundant H$_2$D$^+$ and form D-bearing molecules, and indeed correlation between the amount of CO depletion and the deuterium fractionation (D_{frac}, defined as the abundance ratio between a D-bearing molecule and its hydrogenated counterpart) was found in low-mass dense cores (e.g., Crapsi et al. 2005). Freeze-out of CO and other neutrals has also another crucial implication: frozen on grain mantles, atoms and molecules can undergo hydrogenation (and deuteration), due to the high mobility of the light H (and D) atoms. In particular, from hydrogenation of CO, the most abundant neutral molecule after H$_2$, one forms sequentially HCO, H$_2$CO and CH$_3$OH, which is thus the species that is formed last. Therefore, as time proceeds, the formation of methanol and its deuterated forms (CH$_2$DOH, CH$_3$OD, CHD$_2$OH, etc.) is boosted, until the energy released by the nascent protostellar object in the form of radiation increases the temperature of its environment, causing the evaporation of the grain mantles and the release of these molecules into the gas. As the temperature increases, the deuterated species are expected to get gradually destroyed due to the higher efficiency of the backward endothermic reactions (Caselli & Ceccarelli 2012). Therefore, high D_{frac} of species formed in the gas, like N$_2$D$^+$ and DCN, are good tracers of the pre–stellar phase, while high D_{frac} of methanol are expected to better trace the short-living evolutionary stage in between the pre-stellar and the protostellar phase, at which the evaporation/sputtering of the grain mantles is efficient, and the warm gas-phase reactions have no time to change significantly the chemical composition of the gas. Recent observations of these molecules in dense high-mass star-forming cores belonging to different evolutionary stages

Table 1: Ground rotational transitions of deuterated molecules in ALMA Band 2

molecule	rest freq. (GHz)
DCO^+ (1–0)	72.03931
DCN (1–0)	72.41469
CCD (1–0)	72.09843 – 72.20019
DNC (1–0)	76.30570
N_2D^+ (1–0)	77.10924
$ortho$-NH_2D ($J_{K1K2} = 1_{1,1} - 1_{0,1}$)	85.92772

(Fontani et al. 2015) indicate the essential validity of this scenario.

In this framework, observations of deuterated molecules are crucial to derive the kinematics and other chemical/physical properties of pristine dense cores. This information is mandatory to understand the initial phases of the star formation process and put constraints on current theories. In particular, because of the low temperature, the ground rotational transition (1–0) is certainly the most sensitive probe because it is the easiest line to excite even at very low temperature. However, unfortunately the (1–0) rest frequency of many deuterated isotopologues of common, abundant interstellar molecules is below 80 GHz, not accessible by most of the current millimeter single-dish telescopes and interferometers. For this reason, the large majority of the studies performed so far have used the higher excitation transitions, which are not fully representative of the whole core but just of the densest inner parts. Moreover, the deuterated fractions are often derived by comparing the column density computed from the fundamental transition of the hydrogenated molecule to that derived from higher excitation lines of the deuterated counterpart, which make the ratio dependent on the possibly different excitation conditions. To solve this problem, ALMA Band 2 will be perfectly suitable, because the (1–0) lines of many abundant deuterated molecules, including DCO^+ and N_2D^+, are unique to this band. A list of these lines is reported in Table 1. Also, the excitation temperature of the (1–0) lines can be derived directly from their hyperfine structure, assuming the line to be optically thick. This method in principle is valid also for higher excitation lines, but it is more uncertain because they are expected to be fainter and optically thinner. Finally, in the same single spectral setup one can observe simultaneously many lines of the $ortho$-NH_2D, including the ($1_{1,1}$–$1_{0,1}$) line at ~ 85 GHz, as well as several transitions of HDCO, which can help, all together, to obtain a complete and consistent picture of deuterated molecules in the target cores.

Other important lines that can be observed in Band 2 are those of deuterated methanol, which are important to trace the short-living evolutionary stage in between the pre- and the protostellar phase (see above). Observations of deuterated methanol are possible in several bands, but their identification is difficult at wavelengths shorter than 3 mm because they can be easily overwhelmed by nearby stronger emission lines of lighter and more abundant molecules. Therefore, their detection must be checked carefully with synthetic spectra, which is not an easy task usually (see e.g. Fig. 1 in Fontani et al. 2015). This problem can be bypassed in band 2, because several transitions of CH_2DOH can be observed in the range 67–90 GHz without the contamination of lines of more abundant molecules, as can be seen in Fig. 1. The combination of high angular resolution and high sensitivity offered by ALMA in Band 2 will be eminently suitable to map these lines, which are expected to arise from very compact regions. As an example, we can estimate the time required to detected some of the lines shown in the synthetic spectrum in Fig. 1. The spectrum includes all transitions of CH_2DOH in the spectroscopic band $\sim 67 - 90$ GHz, as modeled by WEEDS assuming the following parameters: $T_{ex} = 20$ K, $N(CH_2DOH)$=5×10^{15} cm^{-2}, source size = 1", line FWHM = 1 km s^{-1}. The column density

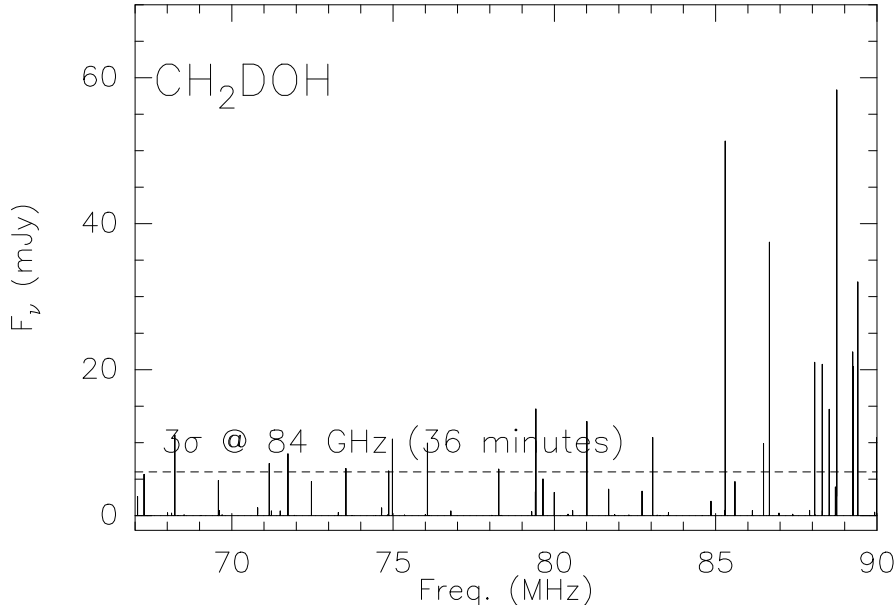Figure 1: *Synthetic spectrum of CH_2DOH modeled with WEEDS in the range $\sim 67 - 90$ GHz, assuming $T_{ex} = 20$ K, $N(CH_2DOH)=5 \times 10^{15}$ cm^{-2}, source size = 1", and line FWHM = 1 km s^{-1}. The dashed line represents the expected 3σ level in the spectrum that can be achieved after 36 minutes of integration on source with ALMA (see text for details).*

assumed is a mean source-averaged value measured towards massive protostellar cores (Fontani et al. 2015). Based on the OT time exposure calculator, at a representative frequency of 84 GHz (the lower frequency currently observed by ALMA), assuming $T_{sys} =60$ K, 36 dishes of 12 m, 2 polarisations, a velocity resolution of ~ 1 km s^{-1}, the 1σ rms noise in the spectrum after just 36 minutes of integration on source is 2 mJy. Fig. 1 tells us that more than 10 lines have intensity peak well above 3σ. Therefore, this will allow us not only to just detect the presence of the molecule in the same spectral setup where the (1–0) lines of the other species will be detected, but also to derive estimates of some important physical parameters from methanol (e.g., gas temperature and column density from the rotation diagrams).

2.4 Understanding the formation of astrobiological molecules

The increasing number of detections of complex organic molecules around young stellar objects strongly suggests that they are part of the material of which planetary systems are made. These molecules play a central role in interstellar prebiotic chemistry and may be directly linked to the origin of life. While the detection of the simplest amino acids such as glycine still remains elusive, the search of two other families of prebiotic molecules has been more successful: aldoses and polyols. The monosaccharide sugar glycolaldehyde (CH_2OHCHO, hereafter GA) is the simplest representative of the aldoses. This molecule can react with propenal to form ribose, a central constituent of RNA (Collins and Ferrier 1995; Weber et al. 1998). The simplest representative of the polyols is the reduced alcohol of GA, ethylene glycol ($CH_2OH)_2$, hereafter EG).

Theoretical chemical models have been developed in the last years to understand how these complex molecules can be formed in the interstelar medium. Woods et al. (2012, 2013) tested six different mechanisms of GA synthesis proposed in the literature, both in the gas phase and on the surface of grains, and concluded that the most likely pathways are 3 grain-surface formation routes involving the formyl radical (HCO):

1) $CH_3OH + HCO \longrightarrow CH_2OHCHO + H$;
2) $H_2CO + HCO + H \longrightarrow CH_2OHCHO$;
3) $2HCO \longrightarrow CO + H_2CO \longrightarrow HOCCOH$;
   $HOCCOH + H \longrightarrow CH_2OCHO$; $CH_2OCHO + H \longrightarrow CH_2OHCHO$.
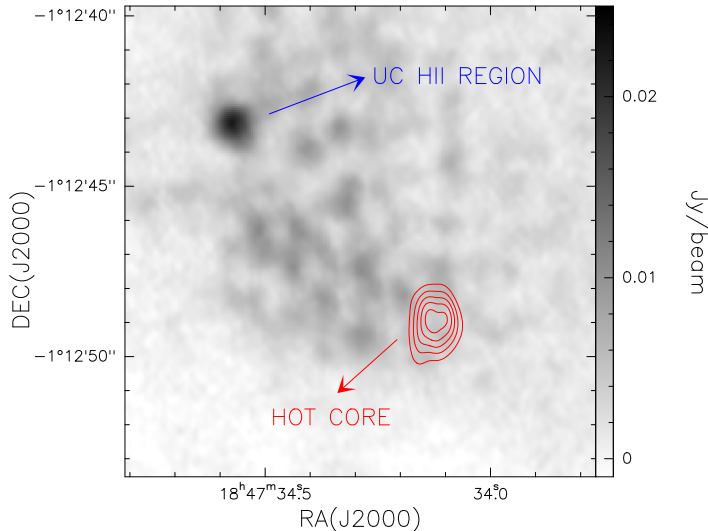

Figure 2: *Integrated intensity of the CH_2OHCHO (GA) line at 1.4 mm (220.46 GHz) detected with PdBI towards the HMC G31.41+0.31 (red contours; Beltrán et al. 2009), overplotted on the VLA map of the 1.3 cm continuum emission (grey scale; Cesaroni et al. 1998). The positions of the HMC and the nearby UC HII region are indicated.*

From a chemical perspective, these proposed formation routes look promising. It is known that HCO is formed on the surface of interstellar grains by the hydrogenation of CO (Woon et al. 2002). Since CO is the secondmost abundant molecule in insterstellar ices, it is expected that the abundance of HCO in the grains is high enough to produce efficiently GA and EG. The third mechanism proposed has been recently supported by the laboratory experiments by Fedoseev et al. (2015). This work also shows that this mechanism is also very efficient in forming EG through sequential hydrogenation by two H atoms: $CH_2OHCHO + H + H \longrightarrow (CH_2OH)_2$.

Interstellar GA and EG were first detected towards the Galactic Center in the SgrB2 region (Hollis et al. 2000, 2002; Halfen et al. 2006). Beltrán et al. (2009) reported the first detection of GA outside the Galactic Center towards the Hot Molecular Core (HMC) G31.41+0.31 (hereafter G31), using the IRAM PdBI (Fig. 2). Recently, the a-conformer of EG, a-$(CH_2OH)_2$), has been detected towards G31 using the IRAM 30m telescope (Fig. 3; Rivilla et al., in preparation). Calcutt et al. (2014) also confirmed the detection of GA towards 5 additional HMCs. Interestingly, GA and EG have also been recently reported towards two low-mass protostellar systems, the binary IRAS 16293−2422 and NGC 1333 IRAS2A (Jørgensen et al. 2012; Maury et al. 2014; Coutens et al. 2015), and towards an intermediate-mass protostar NGC7129 (Fuente et al. 2014). The HCO molecule was first detected in the interstellar medium by Snyder et al. (1976) towards a sample of molecular clouds associated with HMCs.

In agreement with theoretical predictions, very recent single-dish observations suggest a link between HCO, GA and EG. Rivilla et al., (in preparation) has detected for the first time HCO towards G31 using the IRAM 30m telescope. Figure 3 shows the 3 mm spectrum towards G31, including the HCO, GA and EG transitions. Moreover, the spectral line survey by Armijos-Abendaño et al. (2015) towards two Galactic Center molecular complexes has shown that GA is detected only if HCO is also present. These findings support the hypothesis of HCO as a
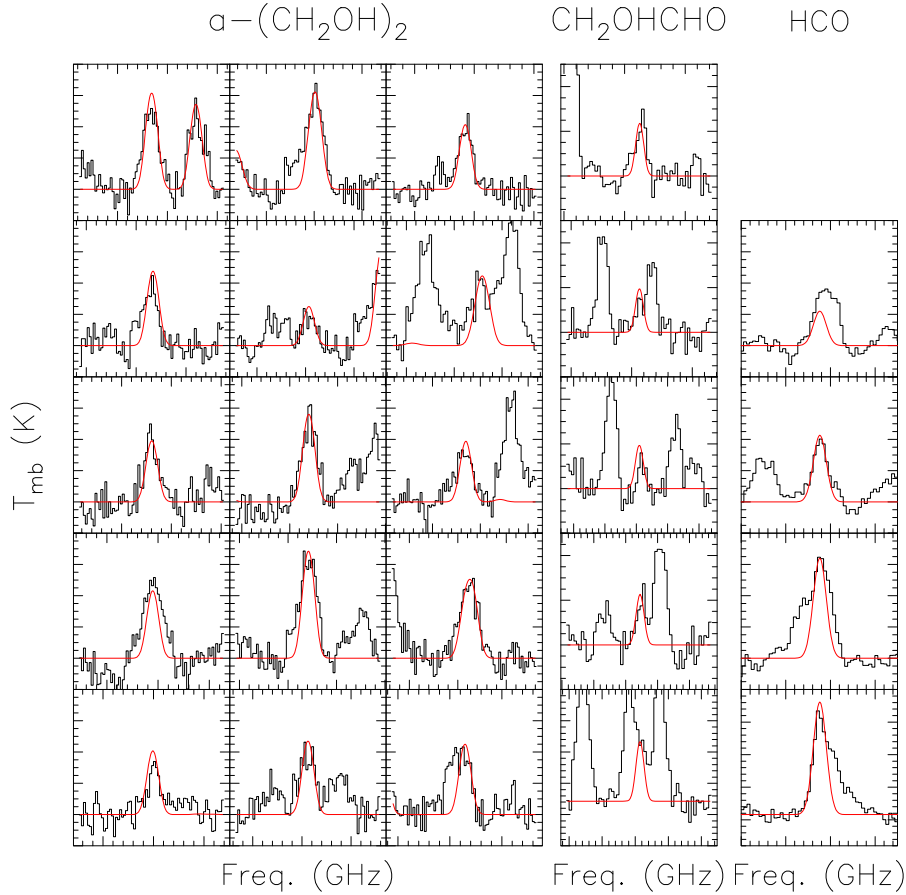
Figure 3: *EG, GA and HCO transitions detected towards G31 HMC with the IRAM 30m telescope (Rivilla et al., in preparation). The red line is the spectrum simulated assuming LTE conditions. The extra emission in the HCO transition in the upper right panel is due to contamination from an unidentified molecule.*

precursor of GA and EG.

2.4.1 Justification for ALMA Band 2+3

The advent of ALMA offers an unprecedented opportunity to study the formation of complex molecules of astrobiological interest in star forming regions. Fig. 4 shows the simulated spectrum of HCO, GA and EG in the ALMA Band 2+3, assuming Local Thermodynamic Equilibrium (LTE) conditions, a temperature of 100 K and the column densities derived from the IRAM 30m detections (Rivilla et al., in preparation). The Band 2+3 will be particularly suitable for the study of complex organic molecules due to several reasons:

- The number of molecular rotational lines excited at these frequencies (67–116 GHz) is significantly lower than at higher frequencies, and hence the transitions of the complex molecules suffer less from line blending with other species.

- The broad frecuency coverage of Band 2+3 will allow us to detect multiple transitions of the molecular species with different excitation energies, which is needed to confirm robustly the detections and to derive the physical parameters (column densities N and temperatures $T_{\rm rot}$).

- The high spatial resolution of ALMA contributes to reduce the line confusion with respect to single-dish observations since different molecules are expected to arise from different regions. If all the transitions attributed to a molecule exhibit the same spatial distribution, the identification is further supported.

- Since the abundance of complex organic molecules is significantly lower than that of simpler molecules, the high-sensitivity of ALMA opens up the possibility to detect a large number of complex molecules that have remained undetected so far.
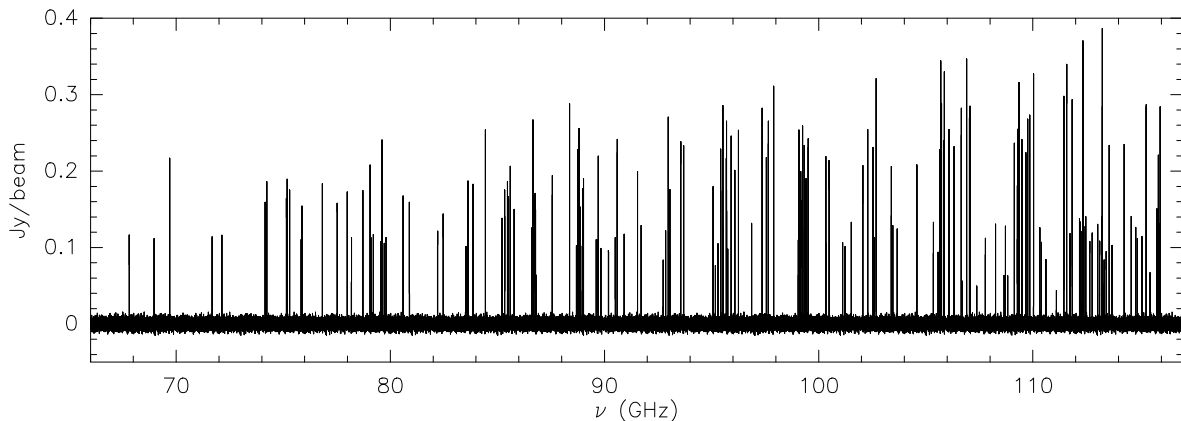

Figure 4: *Simulated spectrum of GA, EG and HCO in the spectral range covered by ALMA Band 2+3 (67-116 GHz), considering the size of the G31 HMC (∼ 1"), a temperature of 100 K and the molecular column densities estimated from the single-dish detections (Rivilla et al., in preparation). The noise provided by ALMA in 30 min hour on-source within beam of 1" is 4.35 mJy/beam, and has been added to the theoretical spectrum.*

2.4.2 Comparison between observations and chemical models

Once the molecular species are clearly identified and its abundances well determined, the comparison with chemical models will shed light about their formation processes. Figure 5 shows the predictions of the suface chemistry on the grains considering the 3 different pathways proposed by (Woods et al. 2012). The different routes predict well differentiated values of the relative surface abundances. Since gas-phase formation of GA and EG is unlikely (Woods et al. 2012), the present gas abundances are expected to be directly linked with the original surface abundances. In the case of HCO, it is also expected that the observed gas abundance is mainly inherited from the abundance in the grains mantles after evaporation (Gerin et al. 2009; Cernicharo et al. 2012). Therefore, the comparison of the observed gas abundances with the chemical models would reveal which of the proposed chemical routes is more likely.

2.5 Complex organic molecules in protostellar environments in the ALMA era

2.5.1 The molecular complexity in a Sun-like forming system

Molecular complexity builds up at each step of the Sun-like star formation process, starting from simple molecules and ending up in large polyatomic species. Understanding how our own solar system, Earth and life, have come to be is one of the most important and exciting topics in science. Complex organic molecules (COMs; such as methyl formate, $HCOOCH_3$, dymethyl ether, CH_3OCH_3, or glycolaldehyde, $HCOCH_2OH$) have been found in all the components of the
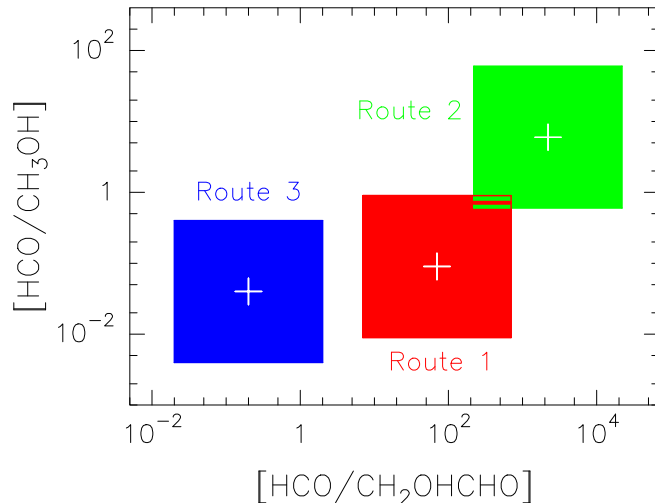
Figure 5: *Theoretical predictions of the HCO, CH$_3$OH and GA abundances from the chemical models by Woods et al. (2012) at the end the surface-chemistry phase, when the complex organic molecules (GA and EG) are formed. A source with the physical conditions of G31 was considered. The colored boxes consider an uncertainty of ±1 order of magnitude.*

star formation recipe (prestellar cores, hot-corinos, circumstellar disks, shocks induced by fast jets). These species are thought to be mostly formed in solid state chemistry of grain mantles and then released in the gas phase due to ice grain mantle sublimation or sputtering, and in some cases enhanced by gas-phase reactions. Intriguingly, the simplest, non-chiral amino acid, glycine (C$_2$H$_5$NO$_2$), has been found in comet and meteorite samples from our own Solar System, but its detection in star-forming regions is still a matter of intense debate. The level of chemical processing and complexity of ices in low-mass star forming regions and protoplanetary disks and their relationship with the material delivered on planetary surfaces is still very uncertain, in spite of the astrobiological implications. The combination of theoretical, observational and laboratory studies has the potential of advancing this field considerably, especially in the ALMA era and with the prospect of expanding the ALMA capabilities to the Band 2 (or 2+3) range.

2.5.2 COMs: from prestellar cores to planetary systems

The formation of Sun-like stars and the chemical complexity of the molecular gas involved in the process can be summarised as follows (see Fig. 6, from Caselli & Ceccarelli 2012): (1) matter slowly accumulates toward the center of a molecular cloud. The central density increases while the temperature decrease. Atoms and molecules in the gas phase freeze-out onto the cold surfaces of the dust grains, forming the grain mantles. Hydrogenation of atoms and molecules takes place, forming molecules such as water (H$_2$O), and formaldehyde (H$_2$CO). The recent detection of COMs in cold cores (e.g., Bacmann et al. 2012) support that in these regions the formation of new molecules in icy mantles is also caused by the effects of UV photons and low-energy cosmic rays; (2) the collapse starts, the gravitational energy is converted into radiation and the envelope around the central object warms up. The molecules frozen on the mantles acquire mobility and form new, more complex species. When the temperature reaches about 100 K the mantle sublimates, given origin to the so-called hot corino phase, which has a very small size (≤ 0.01 pc). Molecules in the mantle are injected in the gas, where they react and form new, more complex, molecules. The abundance of COMs (such as methyl formate, HCOOCH$_3$, or dymethyl ether, CH$_3$OCH$_3$) dramatically increases. A classical example is provided by IRAS16293–2422 (e.g., Ceccarelli et al. 2007), where recently also glycolaldehyde (HCOCH$_2$OH), a crucial molecule
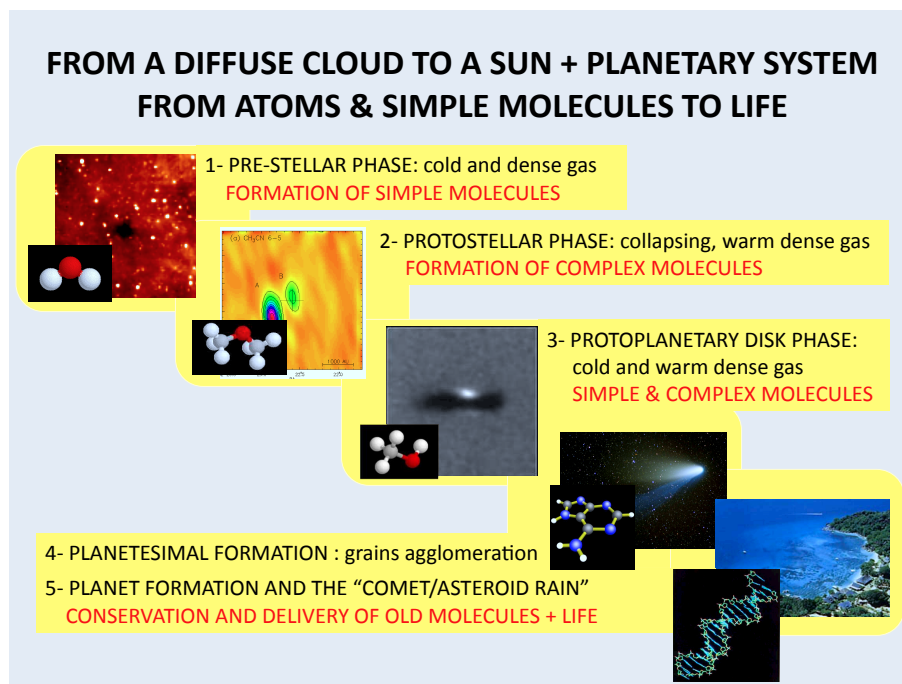
Figure 6: *Star formation and chemical complexity (from Caselli & Ceccarelli 2012). The formation of a star and a planetary system, like the Solar System, passes through different phases, marked in the sketch.*

for the formation of metabolic molecules, has been detected (Jörgensen et al. 2012; see also Taquet et al. 2015); (3) simultaneously to the collapse, a newborn protostar generates a fast and well collimated jet, possibly surrounded by a wider angle wind. In turn, the ejected material drives shocks travelling through the surrounding high-density medium. Shocks heat the gas up to thousands of K and trigger several processes such as endothermic chemical reactions and ice grain mantle sublimation or sputtering (e.g., van Dishoeck & Blake 1998). Several molecular species undergo significant enhancements in their abundances. The prototypical chemical rich shock in a molecular outflow is L1157-B1 (Bachiller et al. 2001). Toward this source, not only relatively simple complex molecules, like methanol, have been detected, but also molecules considered hot corinos tracers, like methyl formate ($HCOOCH_3$), ethanol (C_2H_5OH), formic acid ($HCOOH$) and methyl cyanide (CH_3CN) (Arce et al. 2008; Codella et al. 2009). The emission of these species is concentrated in a small (<1000 AU) region associated with the violent shocks at the head of the outflowing material. The presence of COMs in molecular outflows strongly suggests that these species were part of the sputtered icy mantles, because the time elapsed since the shock is too short for any gas-phase route to build up COMs; (4) the envelope dissipates with time and eventually only a circumstellar disk remains, which is also called protoplanetary disk. In the hot regions, close to the central forming star, new complex molecules are synthesized by reactions between the species formed in the protostellar phase. In the cold regions of the disk, where the vast majority of matter resides, the molecules formed in the protostellar phase freeze-out onto the grain mantles again. Dust grains then coagulate into larger planetesimals, the bricks of future planets, comets, and asteroids.

2.5.3 The IRAM–ALMA synergy

In the last years several large programs started collecting unbiased spectral surveys with high frequency resolutions and unprecedented sensitivities of different targets considered among the typical laboratories of different stages of the low-mass star forming process (as e.g., prestellar cores, hot-corinos, protostellar shocks, more evolved Class I objects). One of the main goals is indeed the detection of complex and rare molecular species in the interstellar space through emission due to their ro-vibrational transitions. In particular, these efforts have been recently carried out in the 80–300 GHz range using the IRAM 30-m ground based observatory (ASAI: Astrochemical Surveys At IRAM; http://www.oan.es/asai) and between 500 GHz and 2000 GHz using the ESO Herschel Space Observatory (CHESS: Chemical HErschel Surveys of Star forming regions; http://www-laog.obs.ujf-grenoble.fr/heberges/chess/).

A huge effort is carried out also using interferometers to provide high-spatial resolution images. The IRAM Plateau de Bure interferometer (PdBI) large program CALYPSO (Continuum and Lines from Young ProtoStellar Objects; http://irfu.cea.fr/Projects/Calypso) is providing the first sub-arcsecond statistical study, in the 80–300 GHz window, of the inner environments of the low-luminosity Class 0 sources. Also in this case spectacular forests of lines are observed, showing an amazing large number of lines at high excitation due to COMs such as glycolaldehyde and ethylene glycol (aGa'–$(CH_2OH)_2$), originating from a region of radius 40–100 AU, centered on the protostar. The collected spectra are very rich in COMs showing amazing forest of lines, reflecting the chemical complexity of all the components involved in the low-mass star formation. A particular case is represented by formamide (NH_2CHO), the simplest possible amide and a central molecule in the synthesis of metabolic and genetic molecules, which has been revealed towards both hot-corinos and protostellar shocks (e.g., Mendoza et al. 2014; López-Sepulcre et al. 2015). Finally, the IRAM NOEMA large program SOLIS (Seed Of Life In Space) started its operations with the goal to provide the first systematic COMs study towards a large sample covering the first phases of Solar-type star formation. The high-resolution images will pin down where COMs are located, their abundances, and how they are influenced by evolutional and environmental factors, shedding light on COMs formation and destruction routes.

In conclusion, the synergy between spectral surveys using single-dishes and interferometric observations is of paramount importance to detect and analyse the COM emission. On the one hand, the unbiased spectral surveys provide the largest possible frequency range, and thus the most complete census of COMs; a multiline approach is also needed to safely identify the emission spectrum of complex species. On the other hand, interferometric images provide the size and morphology of the emitting regions, overcome the filling factor limitation of single-dish spectra, and allow one to propely derive physical conditions such as density, temperature, and abundance. In addition, the linewidths of COMs are typically reduced in interferometric observations, which allows a better identification of the molecular lines since it reduces line blending.

2.5.4 Amino acids in Solar-system precursors

The increasing performance of millimeter instrumentation in the past years has opened up the possibility to carry out high-sensitivity molecular line surveys even toward the earliest (and coldest) stages of low-mass star formation. These initial conditions are represented by cold dark cores and in particular, by pre-stellar cores, i.e., dense and cold condensations on the verge of gravitational collapse (central H_2 densities of some 10^4 cm^{-3} and temperatures $\leq$10 K). These observations have shown that COMs are also present in the cold gas of these cores, unexpectedly revealing a high chemical complexity in these objects (e.g., Bacmann et al. 2012). Among these complex organics, amino acids are of high interest in Astrochemistry and Astrobiology because of their role in the synthesis of proteins in living organisms. It is currently believed that their
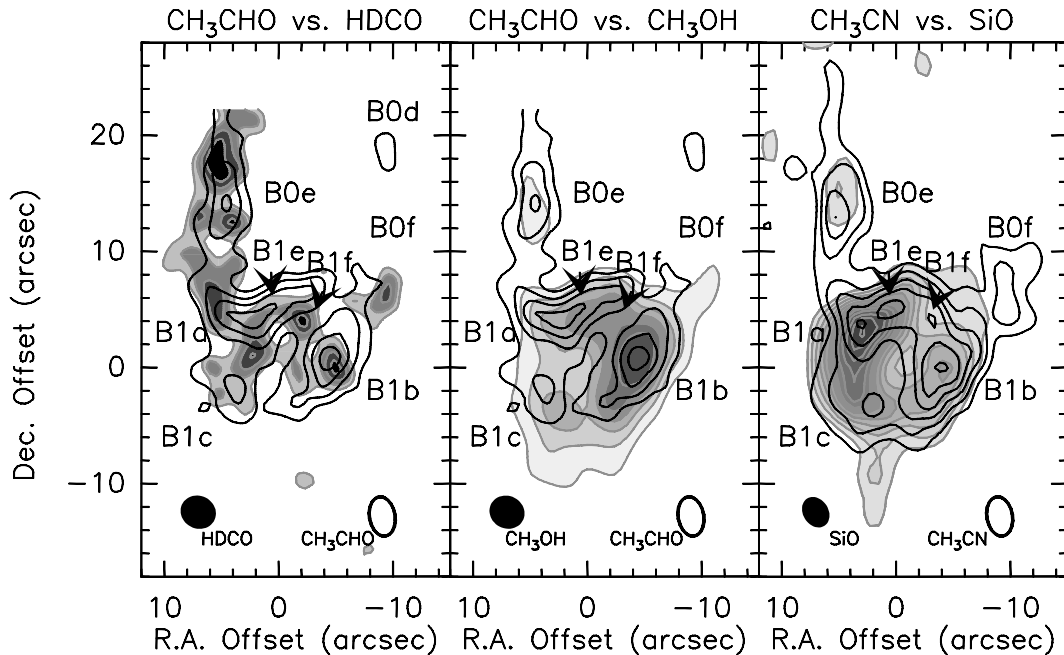
Figure 7: *Chemical differentiation in L1157-B1: the maps are centred at $\Delta\alpha = +21^o$ and $\Delta\delta = -64^o$ from the driving protostar L1157-mm. Overlay of the integrated intensity IRAM PdBI map at 2 mm of the CH_3CHO ($7_{0,7}$–$6_{0,6}$)AE (contours, from Codella et al. 2015) on the HDCO ($2_{1,1}$–$1_{0,1}$) (left panel, from Fontani et al. 2014) and CH_3OH (3_K–2_K) emission (middle panel; from Benedettini et al. 2013). Righ panel compares the CH_3CN (8_K–7_K) and SiO (2–1) spatial distributions (Gueth et al. 1998, Codella et al. 2009). Labels are for the different L1157-B1 molecular clumps well imaged in the CH_3CN map. The synthesised beams are shown in the bottom part of the panels.*

formation may have occurred in the interstellar medium (ISM) since amino acids, including glycine and alanine, have been found in meteorites (e.g., Pizzarello et al. 1991; Glavin et al. 2006) and comets (as in Wild 2; Elsila et al. 2009). However, the detection of amino acids in the ISM remains to be reported.

Recently, it has been proposed that pre-stellar cores may be well suited for the detection of amino acids in the ISM (Jiménez-Serra et al. 2014). The gas temperatures in pre-stellar cores are $\leq$ 10 K, which yields a low level of line confusion since the number of molecular transitions excited at these temperatures is small. The linewidths of the molecular line emission in these cores are $\leq$ 0.5 $\mathrm{km\,s^{-1}}$, which allows accurate identifications of the observed molecular lines because they suffer less from line blending. In addition, water vapour has recently been found toward the central few thousand AU of one pre-stellar core, L1544, which indicates that a small fraction of the ices ($\sim$0.5% of the total water abundance in the mantles) has been released into the gas phase (Caselli et al. 2012). These authors have proposed that water vapour in L1544 is produced by the partial photo-desorption of ices by secondary, cosmic ray induced UV-photons. Since COMs form in the outer layers of the mantles, these molecules are also expected to be photo-desorbed together with water in pre-stellar cores, making these objects excellent candidates to test the detectability of amino acids in Solar-system precursors. The detection of glycine, and of its COM precursors, in these Solar-system precursors will represent a major milestone in Astrochemistry and Astrobiology, providing a unique opportunity to link the pre-biotic chemistry in the ISM to their subsequent delivery onto planetary systems.

2.5.5 Hot protostellar shocks versus hot-corinos

The L1157 region at 250 pc hosts a Class 0 protostar (L1157-mm) driving a spectacular chemically rich bipolar outflow associated with cavities seen in the IR H_2 and CO lines (e.g., Neufeld et al. 2009; Gueth et al. 1996). The bow shocks, when mapped with the IRAM PdB and VLA interferometers, are well traced by typical products of both grain mantle sputtering (such as NH_3, CH_3OH, and H_2CO) and refractory core disruption (SiO). In particular, the bright and young ($\sim$2000 yr) L1157-B1 shock offers an exceptional opportunity to investigate in details the chemical composition of the grain ice mantles as well as how the gas phase is chemically enriched after the shock occurrence.

Thanks to PdBI observations (see Fig. 7), three COMs have been so far imaged in L1157-B1: CH_3OH, acetaldehyde (CH_3CHO), and CH_3CN (Benedettini et al. 2013; Codella et al. 2009, 2015). The CH_3CN image shows a clumpy structure superimposed to the classical B1 arch-like shape, displaying a unique continuous structure tracing the propagation of a large bow shock. Recently, also CH_3CHO has been mapped at PdBI (Codella et al. 2015), and also in this case there is a good agreement with the CH_3OH (and CH_3CN) spatial distribution, confirming COMs are emitting where mantles have been recently sputtered. This is further indicated by the excellent spatial correpondance with HDCO emission (Fontani et al. 2014) tracing deuterated formaldehyde formed on grains and then injected in the shocked gas. For acetaldehyde, the abundance ratio with respect to methanol is quite high ($\sim 10^{-2}$) and in any case similar to that observed towards a typical hot-corino such as IRAS16293–2422 (Bisschop et al. 2008). These findings support for CH_3CHO either a direct formation on grain mantles or a quick (≤ 2000 yr) formation in a chemically enriched gas phase.

These first results show the importance of studying shocked regions as laboratories where (i) to investigate the COMs formation routes and (ii) to verify whether the study of hot-corinos chemistry can be affected by COM emission arising from shocked envelope material at the base of the inner (unresolved) jet. Interferometric observations are instructive to minimise beam dilution effects. In addition, the multiline approach is needed to carefully sample the excitation conditions and correctly derive the abundances of COMs.

2.5.6 Justification for ALMA Band 2+3

The numerous detections of high-excitation COM lines at frequencies larger than 80 GHz call for observations at lower wavelengths, where heavy species are expected to emit (JPL, http://spec.jpl.nasa.gov, and CDMS, http://www.astro.uni-koeln.de/cdms). Even more important, the millimeter frequency bands are often so full of lines that it is paradoxically difficult to identify species through a large number of emission lines simply due to confusion. On the other hand, lower frequency bands are relatively clear, given that low energy transitions of light molecules fall at much higher frequencies. The completion of the results obtained at mm-wavelengths with spectral surveys at lower frequencies will allow one to have the possibility to have, for different species, a large number of transitions, which is needed to reliably detect the largest COMs for which the population is distributed over many energy states, having large partition functions. Figure 8 shows as an example the simulation of the $HCOOCH_3$ and $HCOCH_2OH$ spectrum as expected for ALMA Band 2 modeled with GILDAS-Weeds (Maret et al. 2011) in the range $\sim$ 67–90 GHz, assuming LTE conditions and physical parameters expected in hot-corinos (see e.g., Jörgensen et al. 2012). In particular, if we consider bright lines ($S\mu^2 \geq 1\ D^2$) at low excitation ($E_u \leq 20$ K), then the ALMA Band 2+3 band contains a considerable number of COMs transitions. As an example, the line densities for bright, low-excitation transitions of methyl formate and glycolaldehyde in the 67–116 GHz range is $\sim$ 0.4–0.8 line/GHz, ten times higher than in the 116–350 GHz spectral window.

The COM emission is expected to come from regions at sub-arcsec scale (hot corinos, jets,
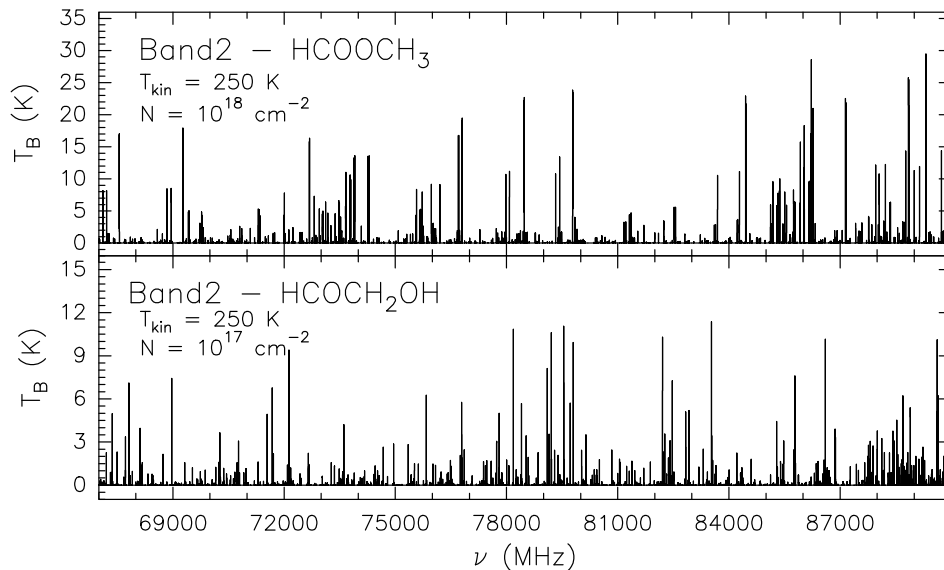
Figure 8: *Simulations of the spectrum of HCOOCH$_3$ and HCOCH$_2$OH as observed by ALMA Band 2 modeled with GILDAS-Weeds (Maret et al. 2011) in the range $\sim$ 67–90 GHz, assuming LTE conditions and physical parameters expected for methyl formate and glycolaldehyde in hot-corinos (see e.g., Jörgensen et al. 2012): $T_{\mathrm{kin}} = 250$ K, $N(HCOOCH_3) = 10^{18}$ cm^{-2}, $N(HCOCH_2OH) = 10^{17}$ cm^{-2}, source size = 1", and line FWHM = 4 km s^{-1}.*

shocks). With a largest baseline of about 16 km, ALMA will provide in Band 2+3 a well suited spatial resolution of $\simeq$ 50 mas. As a comparison, the IRAM NOEMA interferometer currently reaches a synthetisized beam $\sim$ 1 arcsec at 3 mm (the array does not cover frequencies lower than 80 GHz; http://www.iram.fr). In addition, the effective area offered by ALMA will be definitely larger than that available using the IRAM–NOEMA, even in its final 12 antennas configuration ($\sim$ 2100 m^2). Therefore the combination of spatial resolution and sensitivity offered by ALMA is fundamental to resolve and image the emitting region. In this way, (i) we will have bright line emission, and (ii) we will correctly evaluate COMs abundances.

A special case is represented by glycine. Simple radiative transfer calculations towards the L1544 pre-stellar core show that several glycine lines could reach detectable levels (peak line intensities $\geq$10 mK) in the frequency range between 60 and 80 GHz (Jiménez Serra et al. 2014). These calculations assume a solid abundance of glycine in ices of a few 10^{-4} with respect to water, similar to those synthesized in laboratory experiments of UV photon- and ion-irradiated interstellar ice analogs (e.g., Holtom et al. 2005). This solid abundance translates into a maximum gas-phase abundance of glycine of $\sim$ 8$\times$10^{-11} after ice photo-desorption. In Fig. 9, Jiménez-Serra et al. (2012) report the predicted intensities of glycine for the L1544 core, assuming that the gas-phase abundance of glycine remains constant across the core. The detection of glycine, and of its precursors, in these Solar-system precursors will represent a major milestone in Astrochemistry and Astrobiology, providing a unique opportunity to link the pre-biotic chemistry in the ISM to their subsequent delivery onto planetary systems.
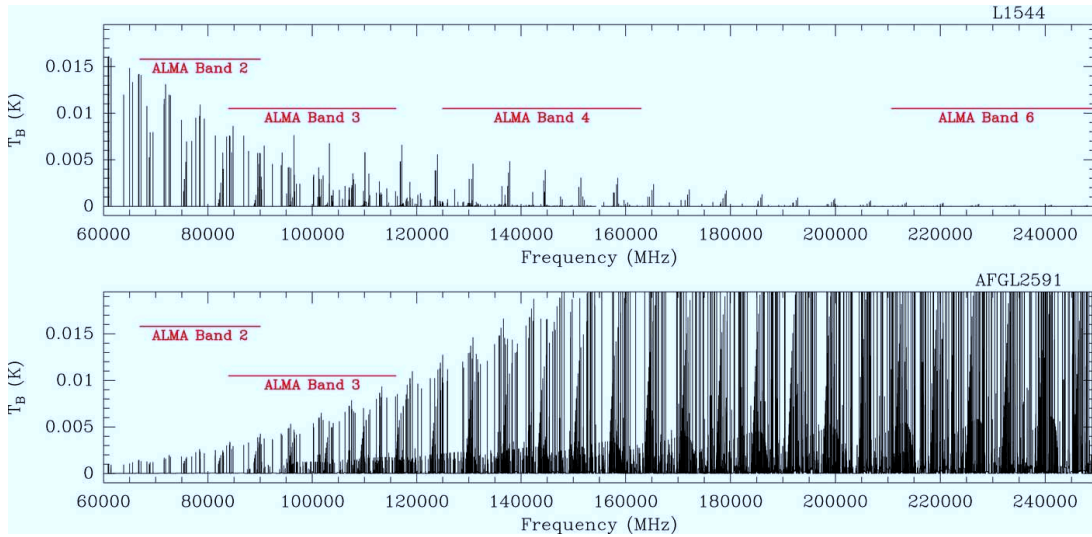
Figure 9: *Upper panel: Simulations of the spectrum of glycine (conformer I) obtained between 60 GHz and 250 GHz, considering the physical structure of the L1544 pre-stellar core (Jiménez-Serra et al. 2012), a solid glycine abundance of a few 10^{-4} with respect to water in ices, and LTE conditions. Horizontal red lines indicate the frequency coverage of ALMA Bands 2, 3, 4, and 6. The glycine lines with frequencies 60–80 GHz show peak intensities $\geq$ 8–10 mK, detectable with the Band 2 receivers of ALMA. Lower panel: LTE spectrum of glycine predicted for the same frequency range (60–250 GHz) but for the AFGL2591 hot molecular core. The glycine lines at 1 mm are brighter than in the pre-stellar core case. However, line confusion and line blending is a major issue in the detection of glycine in hot cores.*

2.6 Chemistry of protoplanetary disks with ALMA Band 2

2.6.1 Protoplanetary disks and the origin of water and organic molecules on Earth and Earth-like planets

Protoplanetary disks are the birthplaces of planets; thus, the study of their physical and chemical structure is fundamental to comprehending the formation of our own solar system as well as that of extrasolar planetary systems. According to our current understanding the primordial disk is composed by μm-sized dust grains which grow and settle towards the midplane forming planetesimal, i.e. bodies from meters to kilometer sizes which are the building blocks of planets, asteroids, and comets (see Testi et al. 2014 for a review on grain growth processes). In the outer cold disk midplane molecules freeze-out onto dust grains covering them with icy mantles. This process is thought to be the first step towards the formation of Complex Organic Molecules (COMs) and prebiotic molecules, which are then inhereted by the forming planetesimal and planets.

One of the main scientific goals of iALMA is to understand the chemistry of COMs and especially their role as building blocks of pre-biotic molecules in exoplanetary systems. There is strong evidence that water on Earth has been delivered after its formation by icy bodies from the outer region of the Solar System pushed inside by the rearrangement of the orbits of the four major planets (Jupiter, Saturn, Uranus and Neptune). These small icy bodies are supposed to have delivered water and other volatiles on the inner rocky planets. As part of this process, complex organic species locked in the ices may have been delivered to Earth as impurities, together with water. Indeed, complex molecules and even simple amino acids, such as Glycine, are known to be present in comets and meteorites, well mixed with water and carbon monoxide ice (e.g., Pizzarello et al. 1991; Glavin et al. 2006).

COMs are thought to form in the interstellar ices around young stars as well as in the ices in circumstellar disks as a consequence of solid-state chemistry induced by energetic radiation from the forming stars (see Caselli & Ceccarelli 2012 for a review). This scenario has been confirmed by laboratory experiments of ice irradiation by energetic particles(e.g., Modica et al. 2010). To date complex organic molecules have been observed at all stages of the star formation process, i.e. in prestellar cores (e.g., Bacmann et al. 2012), in the hot corinos around Class 0 protostars (e.g., Cazaux et al. 2003; Bottinelli et al. 2007), and in the shocks induced by protostellar jets (e.g., Arce et al. 2008; Codella et al. 2009, 2015a). However, the search for COMs in protoplanetary disks has only recently started thanks to the high angular resolution and sensitivity offered by millimeter interferometers such as the Plateau de Bure Interferometer and ALMA.

2.6.2 Chemical complexity in protoplanetary disks

Sub-millimeter and millimeter surveys of disk continuum emission allowed deriving their main physical properties, e.g. the inclination, the size, the dust properties and mass. On the other hand, the disk chemical composition is still poorly known as so far only emission from a few simple molecules has been detected, such as CO, SO, CS, CN, HD, OH, CH^+, HCN, H_2O, CO_2, HCO^+, N_2H^+, C_2H_2, H_2CO, HC_3N (e.g., Bergin et al. 2013, Carr et al. 2008; Chapillon et al. 2012a, 2012b; Dutrey et al. 1997, 2011; Guilloteau et al. 2013; Oberg et al. 2010, 2011; Pontoppidan et al. 2010a; Thi et al. 2004, 2011). The chemical inventory of protoplanetary disks has been very recently enlarged by ALMA observations with the first detection of $c-C_3H_2$ and CH_3CN (Qi et al. 2013b, Oberg et al. 2015; see Dutrey et al. 2014 for a review).

Protoplanetary disks have a stratified structure both vertically and radially with strong gradients in temperature and density as illustrated in Fig. 10 (e.g., Bergin et al. 2007; Dullemond et al. 2007; Dutrey et al. 2014). In the disk surface layers molecules are destroyed due to photodis-
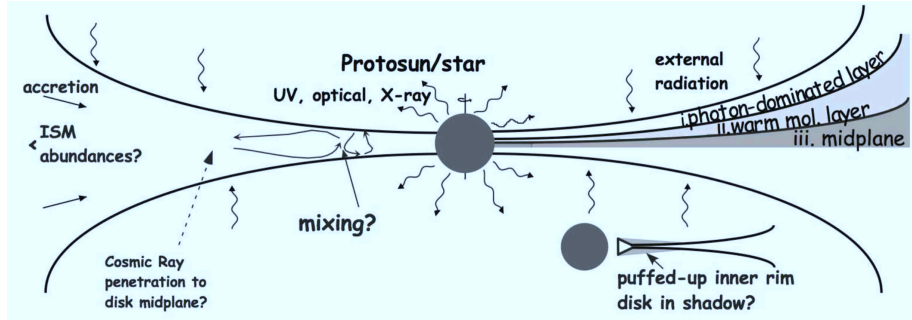
Figure 10: *Chemical structure of protoplanetary disks. Vertically the disk is schematically divided into three zones: a photon-dominated layer, a warm molecular layer, and a midplane freeze-out layer. Various non-thermal inputs, cosmic ray, UV, and X-ray drive chemical reactions. From Bergin et al. (2007).*

sociation by ultraviolet (UV) and X-rays radiation from the central protostar. In the outer disk and close to the disk midplane the temperature quickly drops to $\leq$100 K, therefore molecules freeze out onto dust grains at temperatures determined by their binding energies. Hydrogenated molecules, such as CH_3OH and H_2CO, are thought to be efficiently formed on the grain mantles due to hydrogenation of simple molecules and atoms (e.g., CO, N, C). Then reactions between radicals induced by UV photons or cosmic rays (CR) gives rise to complex organic molecules such as methyl formate (CH_3OCHO) and dimethyl ether (CH_3OCH_3). According to recent protoplanetary disk models, COMs can reach ice-phase abundances of $10^{-6} - 10^{-4}$. However, only a small percentange of those molecules are released in gas-phase by non-thermal processes such as photo- and CR- desoprtion ($\sim 10^{-12} - 10^{-7}$) (Walsh et al. 2014). Hence, the chemical complexity of protoplanetary disks remains basically hidden in their ices making it difficult to observe it.

The recent detection of water (Caselli et al. 2012) and complex molecules (Bacmann et al. 2012) in prestellar cores seems to confirm that COMs can be produced also in cold environments by cold dust grains chemistry and then released by the icy mantles by non-thermal processes. The high densities and low temperature conditions in the cold disk midplane resemble those of pre-stellar cores calling for a deep search of those molecules in protoplanetary disks.

2.6.3 Justification for ALMA Band 2+3

Protoplanetary disks have sizes of a few tens to a few hundreds of AU, i.e. comparable or larger than our solar system. Hence, even for the nearest star forming regions ($\sim$ 100 pc), disks extend on scales $\leq 1''$, therefore high angular resolution is needed to resolve them and to avoid beam dilution. Moreover, as explained above, the abundance of complex molecules in disks is expected to be low ($\sim 10^{-12} - 10^{-7}$) asking for high sensitivity. The ALMA interferometer is the ideal

instrument to search for molecular complexity in protoplanetary disks as the full ALMA array will offer a resolution down to ~ 6 milliarcseconds (which will allow resolving the disk structure down to AU scales for the nearest sources) coupled to very high sensitivity.

In particular, ALMA Band 2+3 will allow us to observe at low frequencies (from 67 to 116 GHz) and to address a number of scientific goals as listed below:

- **The search for complex organic and pre-biotic molecules in protoplanetary disks:** ALMA already proved to be sensitive enough to search for complex molecules in disks, as it recently allowed obtaining the first resolved map of H_2CO in the transitional disk around Oph IRS 48 (van der Marel et al. 2014), the first detection of c-C_3H_2 in the disk around HD 163296 (Qi et al. 2013b), and the first detection of the complex cyanides CH_3CN (and HC_3N) in the disk around MWC 480 (Oberg et al. 2015). As mentioned in Sect. 2.6.2 complex molecules are thought to be formed in large abundances on the icy mantles of dust grains in the cold disk midplane, then partially released in gas-phase due to non-thermal processes, e.g. cosmic rays or UV desorption. In these cool conditions, the rotational spectra of complex molecules is significantly skewed towards low frequencies, as a consequence the detection with ALMA is limited to the lowest bands, e.g. Band 2+3 covering the $67 - 116$ GHz range.

  In particular ALMA Band 2+3 would allow searching for simple amino acids like Glycine (NH_2CH_2COOH) desorbed from icy mantles in disks. Glycine has been found in meteorites and comets of our own Solar System (Oizzarello et al. 1991; Glavin et al. 2006) and laboratory experiments reported the formation of simple amino acids, including Glycine, via ultraviolet and ion photolysis of interstellar ice analogs (e.g., Muñoz-Caro et al. 2002). The recent detection of water vapour in the prestellar core L1544 shows that even in the cold interior of cores cosmic rays and secondary high energy radiation can desorb a measurable quantity of molecules from the ices (Caselli et al. 2012). Jiménez-Serra et al. (2014) have shown that also pre-biotic molecules (like Glycine) may be detectable if desorbed together with the water molecules. In particular, the brightest emission lines can be observed with ALMA Band 2+3 (see Fig. 9 for the predictions of Glycine emission in the prestellar core L1544). We expect that this result can be extended to the cold midplanes of protoplanetary disks.

  The direct detection in the gas phase and measurements of the abundance with respect to water of complex organic molecules would be a significant milestone in studying our cosmic heritage and the ability of ISM and disks chemistry to produce the raw material required for the development of life on exoplanets.

- **The CO snowline:** The snow lines in protoplanetary disks are the condensation fronts where volatiles (e.g. CO, H_2O) freeze-out onto the icy mantles of dust grains. The snow lines are believed to play a crucial role in the formation of planets as the planet formation efficiency and composition are intimately linked to their locations in the disk (see, e.g., Qi et al. 2013a; Pontoppidan et al. 2014). In fact, icy grains located outside the snow line have higher mass surface densities and stickiness compared to bare grains, which favors dust coagulation and particle growth, thus enhancing the efficiency of planet formation. Moreover, the pile-up of dust grains in pressure traps just inside the snow line could allow the grains to grow beyond the radial drift and fragmentation barrier up to planetesimal size. The unprecedented angular resolution offered by ALMA allows us to locate the snow lines in protoplanetary disks around young solar-analogs by observing continuum emission at different wavelengths (e.g., Guidi et al. in preparation) or by means of the so-called chemical rings. For example, the CO snowline can be traced by molecular ion which are present in large abundance where CO is frozen out, e.g. DCO^+ (Mathews et al. 2013) and
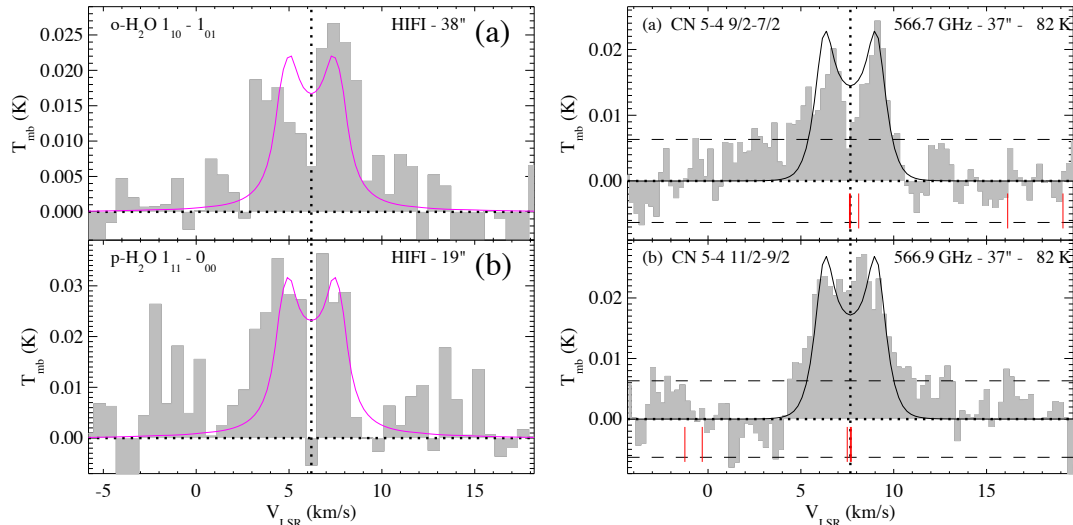
Figure 11: *Left panel:* Water emission from the outer region of the disk of DG Tau. The detected water vapour implies a water reservoir on ices of thousands to hundred thousands Earth Oceans (from Podio et al. 2013). *Right panel:* The embedded disk of T Tau N traced by high-excitation CN (5–4) lines (from Podio et al. 2014a).

N_2H^+ (Qi et al. 2013a). Interestingly the lowest transition of N_2H^+ (the 1–0 transition) is at 93.2 GHz; therefore ALMA Band 3 observations allow a statistical study of the CO snowline in a large sample of protoplanetary disks.

- **Water distribution and deuteration ratio in protoplanetary disks:** Water distribution and deuteration ratio (HDO/H_2O) in protoplanetary disks is key to understand its origin on Earth and to test the scenario of water delivery on Earth by icy bodies from the outer regions of the Solar System, such as asteroids and comets (e.g., Matsui et al. 1986; Morbidelli et al. 2000; Pontoppidan et al. 2014; van Dishoeck et al. 2014). Recently *Herschel* allowed to detect for the first time cold water vapour in the outer regions of protoplanetary disks around young solar-analogs, implying a water reservoir trapped on the icy mantles of dust grains of thousands to hundred thousands Earth Oceans (Hogerheijde et al. 2011; Podio et al. 2013) (see Fig. 11). The observations obtained with *Herschel*, however, are spatially unresolved. To obtain spatially resolved images in the HDO and $H_2^{18}O$ lines is key to validate the scenario of water delivery, as it allows to (i) investigate the radial distribution of water in disks, (ii) to measure the D/H ratio of water in the disk, i.e. the HDO/H_2O abundance ratio. The D/H ratio of Earth Ocean's water (1.5576×10^{-4} 'Vienna Standard Mean Ocean Water', VSMOW or SMOW) is at least a factor of 6 higher than the protosolar nebula value (2.5×10^{-5}: Robert et al. 2000), i.e. of the D/H ratio of the gas out of which our solar system formed. Thus, there should have been an enhancement of the D/H ratio in water at some stages during the solar system evolution. Indeed, the Earth Ocean's HDO/H_2O ratio is similar to what measured in carbonaceous chondrites from the outer asteroid belt (Dauphas et al. 2000) and recently in Jupiter-family comets (Hartogh et al. 2011), while it is a factor two lower than in Oort Cloud comets (Mumma et al. 2011). This suggests that both asteroids and comets may have contributed to delivering water to our own Earth during the Late Bombardment phase(Morbidelli et al. 2000; Hartogh et al. 2011). On the other hand, the HDO/H_2O ratio measured in our solar system (Earth, asteroids, and comets) is much lower than what measured in the cold outer regions of protostellar envelopes ($HDO/H_2O \sim 10^{-2} - 10^{-3}$, e.g. (Coutens et al.

2012, 2013) but similar to the ratio in the warm inner envelope (HDO/$H_2O \sim 3-5 \times 10^{-4}$, e.g. Jörgensen et al. 2010; Persson et al. 2014). Therefore, it is still not clear whether the D/H ratio in the solar system water was already set by ices in the early (pre-)collapse phase and transported largely unaltered to the comet-forming zone, or whether further alteration of D/H took place in the solar nebula disk. ALMA Band 2 should allow us to answer the open questions about the origin of water on Earth as it will allow observing at high resolution and sensitivity one of the lowest transitions of HDO, the $1_{1,0} - 1_{1,1}$ at 80.6 GHz (Note that this line is not covered by the IRAM telescope).

Besides the listed scientific cases, the ALMA Band 2+3 also covers other molecular transitions which can help our understanding of protoplanetary disks chemistry, e.g.:

- the lowest transition of CN (the 1–0 line at 113 GHz, $E_{up} \sim 5$ K). CN has proved to be an efficient tracer of protoplanetary disks (e.g., Chapillon et al. 2012a; Guilloteau et al. 2013; Podio et al. 2014a) (see Figure 11);

- the SO $2_2 - 1_1$, $3_2 - 2_1$, $4_5 - 4_4$, $2_3 - 1_2$ lines falling between 86 and 109 GHz ($E_{up} \sim 9-21$ K). SO is a key molecule to understand the chemistry of sulfur-bearing molecules but is hard to detect in protoplanetary disk (Fuente et al. 2010; Dutrey et al. 2011; Guilloteau et al. 2013). On the other hand, recent studies suggest that SO can probe the accretion shock occuring at the interface between the envelope and the disk in Class 0 protostars (Lee et al. 2014; Sakai et al. 2014; Podio et al. 2015).

While to detect forming disks around young protostars (Class 0, I) requires to observe high excitation transitions of those molecules to avoid confusion with the emission from the surrounding envelope and/or jets (e.g., Podio et al. 2014a, 2015; Sakai et al. 2014), the lowest transitions of CN and SO can be efficiently used to image the evolved disks around Class II and III sources (e.g., Chapillon et al. 2012a; Guilloteau et al. 2013).

2.7 Constraining the nature of flares from young stars in the millimeter regime

2.7.1 Flare events from young stars

High energy processes during the first evolutionary stages of star formation are responsible for both centimeter/millimeter and X-ray emission (Feigelson & Montmerle 1999). Low-mass pre-main sequence (PMS) stars are well known strong X-ray emitters. Their enhanced magnetic activity with respect to more evolved stars produces violent reconnection events in the corona of the stars, where the plasma heated to high temperatures strongly emits variable X-ray emission. Our understanding of the X-ray emission from young stars has dramatically increased in the recent years due to Chandra and XMM-Newton (Getman et al. 2008, Arzner et al. 2007). X-ray observations have revealed thousands of PMS stars in tens of stellar clusters, resulting in good constraints on their X-ray properties such as plasma temperatures, levels of variability, luminosities and X-ray flare rate (e.g., Wolk et al. 2005).

In contrast, the physics associated with the cm/mm events (nature and origin of the emission, variability, timescales, flaring rate) are still poorly constrained. Drake & Linsky (1989) proposed that these flares might be produced by the same coronal activity that is responsible for bright X-ray emission (see review by Güdel 2002). It would be expected then that electrons spiraling in the magnetic field of the corona produce non-thermal and highly variable gyrosynchrotron radiation. Moreover, ionized material in the vicinity of stars, in circumstellar disks or envelopes or at the base of bipolar outflows, also produce thermal free-free (bremsstrahlung) radiation.

Although long-term centimeter variability on timescales of months to years has been observed in star-forming regions (Felli et al. 1993; Zapata et al. 2004; Forbrich et al. 2007), it is still not
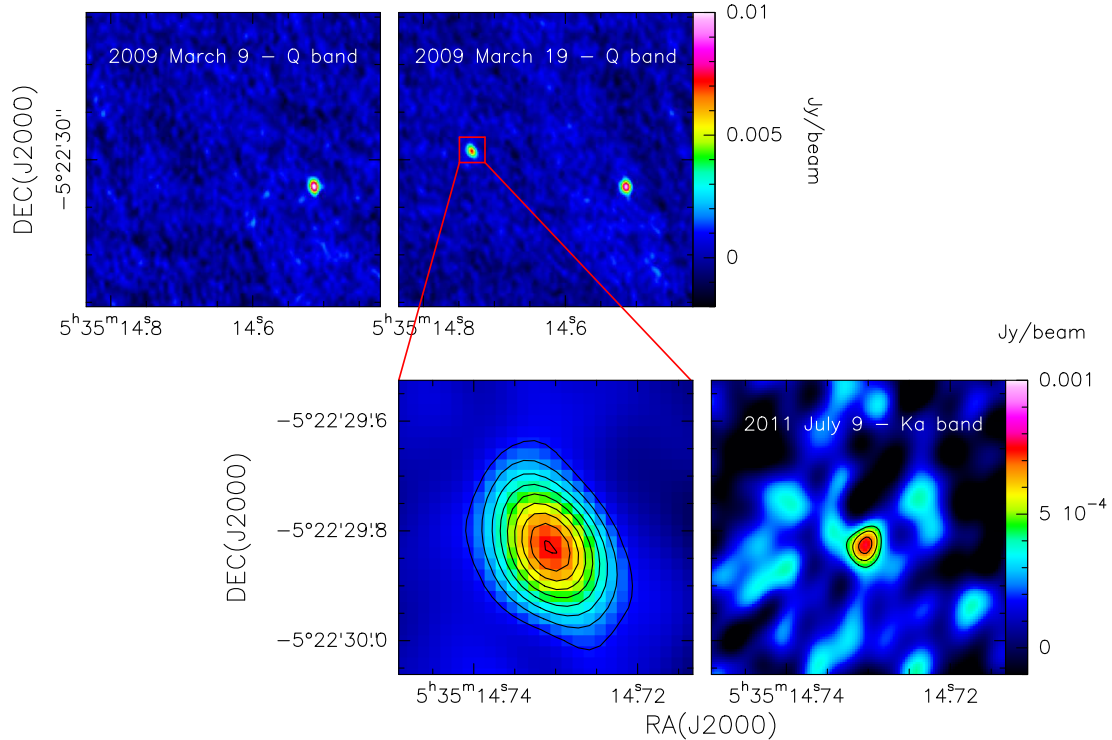
Figure 12: *(Upper panels): Very Large Array (VLA) observations of the Orion Hot Core region at 7 mm from 2009 March 9 (left) and 2009 March 19 (right), from Rivilla et al. (2015). The well known massive source I is detected in both images, while a new centimeter flaring source OHC-E appeared 3.3″ toward the northeast on 2009 March 19. (Lower left panel): Zoom-in view of the detection of the source OHC-E from the 2009 March 19 observation. (Lower right panel): Second detection of OHC-E, from a 9 mm observation carried out in 2011 July 9.*

fully clear that these variations are caused by long-term mechanisms. In the last years it is becoming clear that they may be the result of a continuous sequence of events occurring on shorter timescales. Systematic observations looking for short-term variability are required to answer this question. Recently, Rivilla et al. (2015) have detected a new flaring centimeter source embedded in the Orion Hot Core region (Fig. 12) using the Q-band (7 mm) of Very Large Array (VLA). The source remains below the sensitivity of the observation (∼0.4 mJy) at 2009 March 9, and appeared ten days later with a flux of 8 mJy. A subsequent monitoring of 11 epochs using the Ka band (9 mm) detected this source only once (lower right panel of Fig. 12), confirming that the source is highly variable. This work has also confirmed that the variability from young stars occurs in timescales down to hours towards several sources (Fig. 13). Liu et al. (2014) also detected centimeter variability on hour timescales in the young stellar cluster R Coronae. However, only a few serendipitously detected impressive flares with a good flux density curve have been reported so far (e.g. Forbrich et al., 2008; left panel of Fig. 14).

The low number of observed events have prevented a good undestanding of these flares. Comparing the centimeter and X-ray populations, Forbrich et al. (2013) and Rivilla et al. (2015) have found that the centimeter detections correspond to the brighter X-ray stars. This suggests that the observations at long wavelengths have been strongly limited by sensitivity. The new Karl Janky Very Large Array (JVLA) and ALMA are capable now to significantly increase the number of cm/mm detections of flares from young stars.
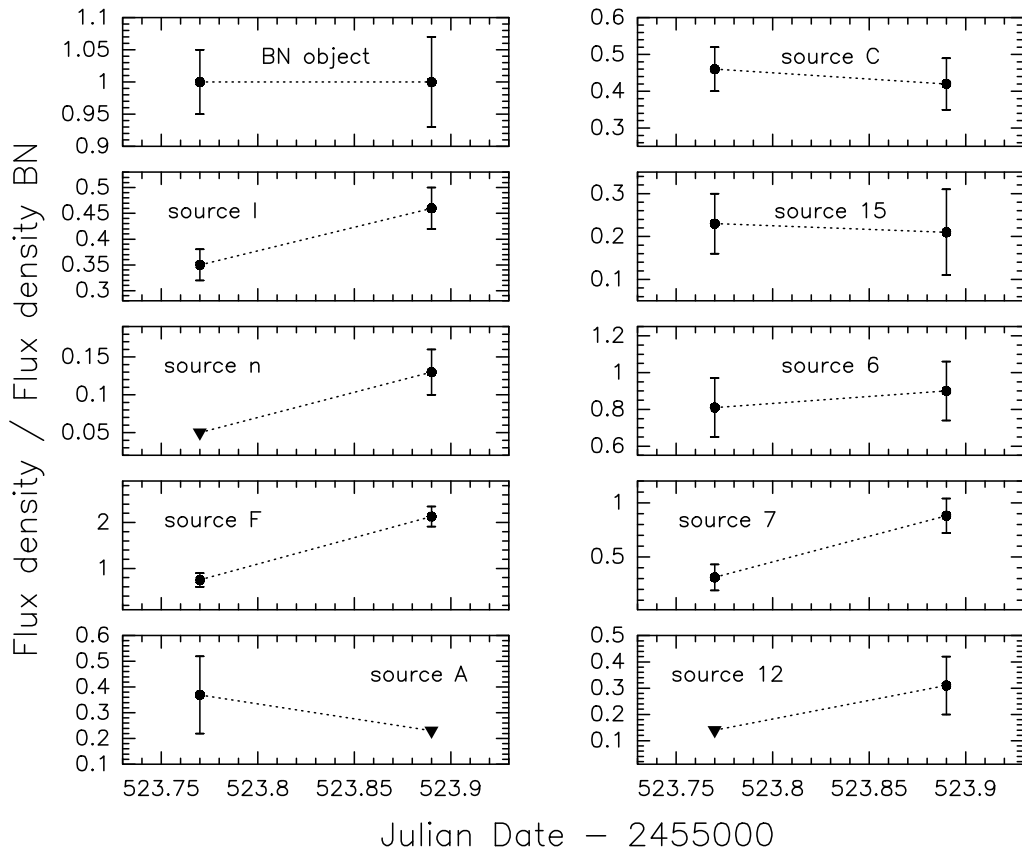
Figure 13: *9 mm flux density variations (normalized by the flux density of the constant massive source BN) on hour timescales for sources of the Orion Nebula Cluster, from Rivilla et al. (2015). The two observations are separated by only 3 hours.*

2.7.2 A new window on high-energy processes in young stellar objects: millimeter-wavelength flares seen with ALMA

ALMA will allow us to study these stellar flares in the millimeter range. The number of flares detected with millimeter instruments so far is very low (e.g. Bower et al., 2003; or Massi et al. 2006, see Fig. **??**). The unprecedented sensitivity of ALMA will surely provide a large number of detection of flares. But ALMA observations not only will allow us to merely expand previous centimeter studies to shorter wavelenghts, but also they will open up a new window of very high-energy processes in young stellar objects. While the centimeter range is probing gyrosynchrotron radiation from mildly relativistic electrons, even greater electron energies (MeV) are accessible in the millimeter wavelength range, where synchrotron radiation from relativistic electrons can be observed. Millimeter-wavelength observations thus probe electron energies that are orders of magnitude above those of stellar X-ray flares. While both gyrosynchrotron and synchrotron radiation can occur in the same source, it is not clear whether they are correlated, and even the centimeter range is thus providing different windows on different physical processes when going from centimeter to millimeter wavelengths. The relativistic electron population causing the synchrotron emission may be entirely independent of its lower energy counterpart, as has been observed on the Sun, where millimeter gyrosynchrotron flares without centimeter counterparts have been observed (e.g., Kundu et al. 2000). With unprecedented sensitivity in the millimeter range, ALMA is thus providing us with a new window on high-energy processes, providing
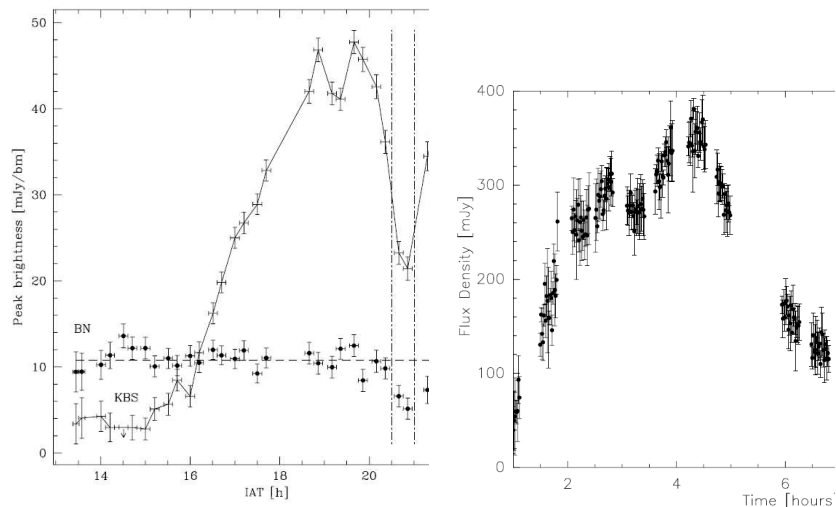
24

Figure 14: *Left:* Light curves at 22 GHz of the Orion flaring source RBS (solid line) and the BN source (circles), detected with VLA (Forbrich et al., 2008). *Right:* Powerful millimeter flare (90 GHz) towards the pre-main sequence binary system V773 Tau A observed in 2003 August 6 with the Plateau de Bure Interferometer (Massi, Forbrich, et al. 2006).

systematic access to very high energy electrons for the first time. ALMA will allow us to test acceleration physics in extremely active stars that may accelerate particles for much longer periods and to much higher energies than the Sun.

ALMA Band 2+3: Nature of the flaring emission from wide band spectral indeces   To constrain the nature of the millimeter flaring emission, a good determination of the spectral indeces (i.e., how the flux density changes with the frequency) will be crucial. Since these events are highly variable in very short timescales, simultaneous observations with high sensitivity in time bins of a few minutes and covering a wide frequency band are required. The ALMA Band 2+3 will suffice these two conditions, since it will allow us to observe simultaneously several spectral windows spanning a wide frequency range between 67 and 116 GHz. This will result in a robust derivation of quasi-instantaneous spectral indeces of the flares, and thus in a good determination of the nature of the emission.

mm-VLBI+ALMA: Revealing the geometry of millimeter flares   The catalogues of millimeter flaring sources that ALMA will provide in the several years will allow us to select the best potential sources to study in detail with millimeter Very long Baseline Interferometry (mm-VLBI) including ALMA. Only such observations will provide the needed sensitivity and spatial resolution to resolve the small-scales (<0.1 AU; << 1 mas) where the flaring emission is expected to be originated. These extremely high resolution images will tell us the geometry of the flares: do they arise directly from the star or alternatively are originated in magnetic loops connecting central star and the circumstellar disk (Feigelson & Montmerle 1999)? Furthermore, these studies will give us a much improved understanding of the high-energy irradiation of protoplanetary disks and its impact on planet formation, including ionization and dissociation. This is key because the high energy environment not only ionizes and dissociates molecules over parts of the disk, but also drives magneto-rotational instability inside them and thus influences the evolution of exoplanet atmospheres.

3 Extragalactic Science

3.1 Dense gas and CO in galaxies with ALMA Band 2

In the context of galaxies in the Local Universe and beyond, there is a unique top-level science driver made possible by ALMA Band 2: characterizing the cool and dense gas in the crucial redshift range $(0.4 \lesssim z \lesssim 2)$ where strong evolution is occurring in galaxy populations.

3.1.1 Low-J CO lines and the redshift desert

Although the power of ALMA as a "redshift engine" has been clearly demonstrated (e.g., Swinbank et al. 2012; Weiss et al. 2013; Simpson et al. 2014), arguably ALMA's greatest contribution will be to characterize the cool gas content of galaxies over the epoch of galaxy formation from $z \gtrsim 8$ down to nearby galaxies in the Local Universe. The epoch of galaxy formation is most commonly traced by the cosmic star-formation rate density of the Universe (SFRD). The SFRD peaks at $z \sim 1-3$, during a period usually associated with the main epoch of galaxy assembly. In this epoch, roughly half of the stars present in galaxies today are formed (e.g., Shapley et al. 2011). The SFRD then declines dramatically toward lower redshift, by roughly an order of magnitude, from $z \sim 2$ to $z \sim 0$, with the most significant decrease at $z < 1$.

One of the most important diagnostics of the epoch of galaxy assembly and the successive decline of the SFRD are observations of cool gas. Theory predicts and observations confirm that the molecular gas fraction increases with lookback time, by as much as a factor of 7 from $z = 0$ to $z \sim 2$ (e.g., Schaye et al. 2010; Daddi et al. 2010; Tacconi et al. 2010; 2013; Lagos et al. 2011; Genzel et al. 2015). At $z \sim 2$, molecular gas can contribute $60-70\%$ to the total baryonic inventory. Such a high gas content and the decline in gas mass fraction toward lower redshifts is undoubtedly associated with the peak of the SFRD, and its decrease toward the present day. The epoch from $z < 1$ is thus crucial to understand why galaxies exhausted their fuel for star formation in the latest stages of the age of the Universe.
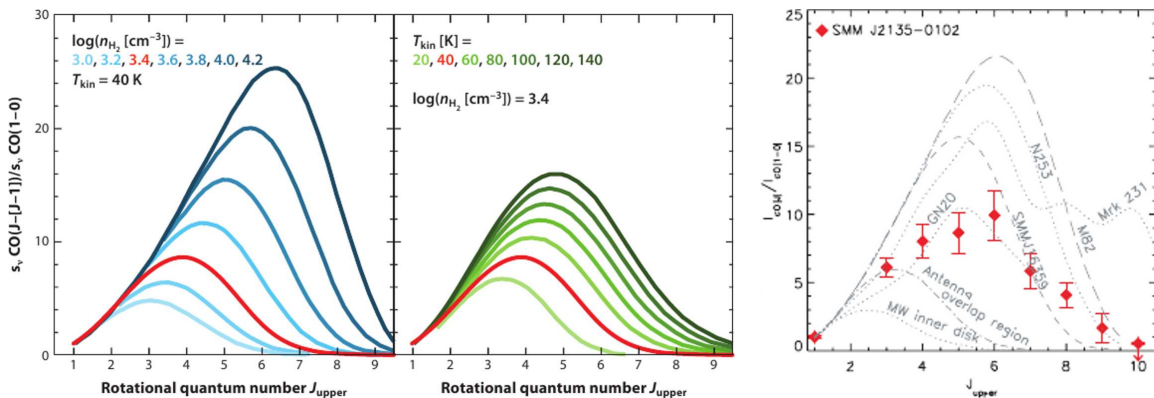

Figure 15: *Left: Theoretical CO Spectral Line Energy Distributions (SLEDs) for different physical conditions, taken from Carilli et al. (2013). Right: Integrated CO SLED for a sub-millimeter galaxy (SMG), SMM J2135-0102 at $z = 2.3$, taken from Danielson et al. (2011). The gray curves show observed SLEDs from different galaxies, illustrating the contrast between starbursts such as NGC 253 and M 82, and more quiescent systems such as the Milky Way inner disk.*

Recent years have seen the number of high-z galaxies with molecular gas-mass estimates increase exponentially. However, uncertainties in two critical factors still hamper the interpretation of observations: one is the large uncertainty in X_{CO}, the factor that converts observed

CO column densities to H_2 masses. This factor depends on physical conditions in the molecular clouds, including density, temperature, radiation field, and metallicity, and can vary by a factor of 50 or more over the variety of galaxy populations that dominate the SFRD at $z \sim 0-3$ (see Bolatto et al. 2013, and references therein). Ultimately, assumptions are made based on observations of a single CO transition, but the more varied galaxy populations and different physical conditions at high redshift make X_{CO} highly uncertain.

The other uncertainty is linked with the necessity, up to now, of observing high-redshift galaxies in high-J CO transitions. Most of the observations of gas in high-z galaxies have been carried out in CO (3–2) or higher-J lines (e.g.., Daddi et al. 2010; Tacconi et al. 2010; 2013). However, the estimate of gas masses is ultimately based on the CO (1–0) transition, so that ratios of the higher-J lines relative to 1→0 must be assumed. As illustrated in the left panel of Fig. 15, these ratios are critically related to excitation conditions, and the temperature and density in the molecular clouds. Physical conditions are known to vary between low- vs. high-SFR galaxies, and compact vs. extended star-forming regions (e.g., Weiss et al. 2005; Danielson et al. 2011), as illustrated in the right panel of Fig. 15. *Observing only high-J lines skews mass estimates toward the warm, dense gas traced by these transitions, and can cause molecular gas masses to be severely underestimated* (e.g., Narayanan et al. 2009; Dannerbauer et al. 2009; Aravena et al. 2010; Ivison et al. 2011).

3.1.2   Band 2 and cool gas mass

Band 2 can mitigate, if not completely resolve, these uncertainties. CO (1–0) is unobservable at $z > 0.3$ with only Band 3, and CO (2–1) is recovered by Band 3 only at $z \sim 1.0$. However, Band 2 enables CO (1–0) measurements over this crucial range in redshift, from $z \sim 0.3$ to $z \sim 0.7$ where SFRD falls dramatically and the Universe is about 3/4 of its present age ($0.3 < z < 1.0$ corresponds to lookback times from 3.4 Gyr to 7.7 Gyr). Figure 16 illustrates the CO ladder and the band coverage as a function of redshift. From $z = 0.29$ to $z = 0.72$, Band 2 combined with the other ALMA bands enables observations of between seven and nine transitions, including the four with lowest J; Band 2 covers 1→0, thus making possible a complete assessment of excitation conditions and the CO spectral line energy distribution (SLED).
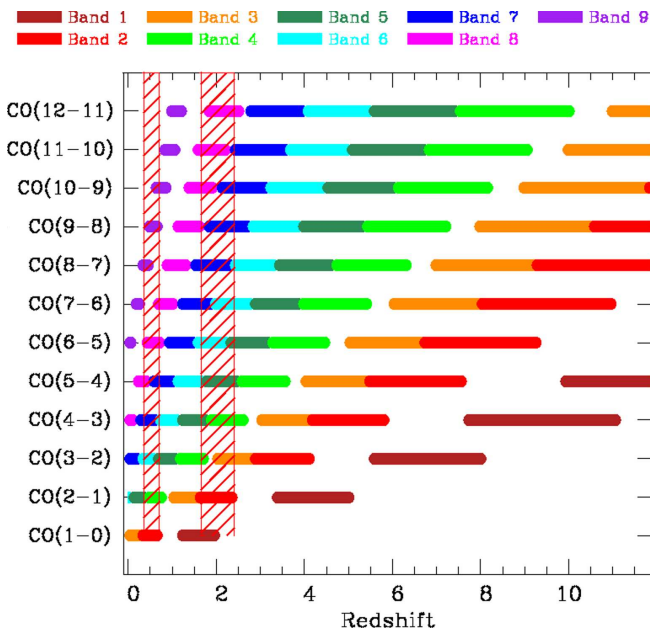

Figure 16: *CO ladder coverage by the ALMA receivers plotted against redshift. The vertical hatched strips show the potential of ALMA with Band 2 to measure multiple transitions in two crucial redshift regions, the first where the Universe is 3/4 of its present age, and the second where the cosmic SFRD peaks.*

No CO lines can be observed in Band 1 until $z \sim 1.2$, where the (1–0) transition enters
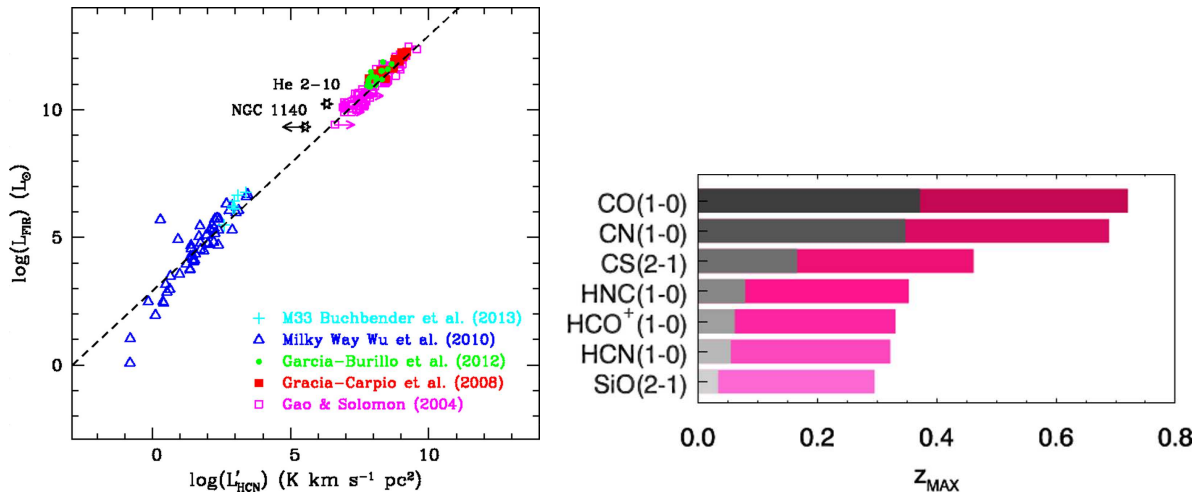
Figure 17: *Left: Correlation between the star formation rate (traced by total IR luminosity) and HCN luminosity in a sample of nearby galaxies, taken from Hunt et al. (2015, in prep.). Right: Molecular transitions of interest for studying dense gas, plotted as a function of the maximum redshift at which they are detectable with ALMA. Grey bars show the current possibilities, and pink bars indicate the improvement that can be achieved with Band 2 (Image courtesy of C. Cicone; taken from the European Science Case for ALMA Band 2: Fuller et al., in preparation).*

the band; Band 2 recovers CO (2–1) at $z \sim 1.6$ which remains observable with Band 2 until $z \sim 2.4$. Thus, in the redshift range where the SFRD is peaking, from $z \sim 1.6$ to $z \sim 2.4$, Band 2, together with the other ALMA bands, provides coverage of between eight and eleven CO transitions; Bands 2+1 measure the two lowest-J transitions, indispensable for accurate gas mass estimates. As shown in Fig. 15, such band coverage is fundamental because of the shape of the CO cooling curve, which peaks around 6→5 in the case of starbursts, or toward lower J in the case of more quiescent disks. The factor to scale the higher-J lines to 1→0 depends on excitation, and is virtually impossible to estimate without multiple transitions.

Expanding the frequency coverage of ALMA by installing Band 2 (or 2+3) will allow the almost complete exploration of the cool gas content in galaxies in this important stage of the age of the Universe. There would remain only a gap of ~ 0.7 Gyr in the evolution of the Universe (between $z \sim 0.84$ and $z \sim 1$, where CO (2–1) shifts out of Band 4 and into Band 3; CO (1–0) is recovered by Band 1 at $z \sim 1.2$). These low-J transitions are fundamental to accurately estimate the cool molecular gas mass. As described below, this epoch in redshift is crucial for observationally constraining the physical mechanisms which quench star formation and cause galaxies to transform from blue star-forming systems to "red and dead" ones.

3.1.3 Dense-gas diagnostics of physical conditions in galaxies

Although observations of CO line emission are an effective means of studying the cold molecular gas reservoir in the interstellar medium (ISM) of high-redshift galaxies, it is not directly related to star formation. The dense molecular gas ($n_{H2} \gtrsim 10^5$ cm^{-3}) more directly associated with star-formation is best studied through observations of higher dipole moment molecules with higher critical densities, such as HCN, HNC or HCO$^+$. The luminosity in the HCN (1–0) line is known to correlate tightly with infrared (IR) luminosity (equivalently star-formation rate, SFR) in nearby galaxies (Gao et al. 2004; Wu et al. 2010; Garcia-Burillo et al. 2012). As shown in Fig. 17, this linear correlation extends over almost 10 orders of magnitude, from the IR luminosities of dense Galactic molecular cloud cores ($L_{IR} \gtrsim 10^2$ $L_\odot$) (Wu et al. 2005; 2010) to

luminous IR galaxies ($L_{IR} \gtrsim 10^{11} L_{\odot}$) (ULIRGs: Gao et al. 2004; Garcia-Burillo et al. 2012). Beyond $L_{IR} \sim 10^{11} L_{\odot}$, the correlation becomes super-linear, implying some change in the physical conditions in the galaxy's ISM (Juneau et al. 2009; Garcia-Burillo et al. 2012). As this dense gas in our own Galaxy is generally associated with sites of ongoing star-formation (indicated by the IR luminosity), it is believed that the presence of strong HCN (1–0) line emission in a high-redshift galaxy may be interpreted as coming from the dense gas dominating an ongoing starburst (e.g., Juneau et al. 2009). By comparing the dense gas masses estimated from HCN (1–0) with the total molecular gas masses estimated from low-J CO line emission (e.g., Aalto et al. 1995), the dense fraction and its variation in galaxies can be estimated over cosmic time. Similarly, the dense gas mass can be compared to the SFRs in order to estimate a true star-formation efficiency. As the number density of IR-luminous star-forming galaxies increases with redshift, surveys of HCN (1–0) with Band 2 would provide the only means of constraining the apparent non-linearity at the highest end of the $L_{IR} - L'_{HCN}$ relationship. Molecular line surveys(e.g., Costagliola et al. 2011) with Band 2+3 will be fundamental for efficiently constraining physical conditions in star-forming galaxies up to $z \sim 0.5$.

Figure 17 also shows two galaxies which deviate from the global trend: these are dwarf galaxies He2−10 (Santangelo et al. 2009) and NGC 1140 (Hunt et al. 2015, in prep.). In these galaxies, HCN is under-luminous, almost certainly a result of different physical conditions in their nuclei including low metallicity (Meijerink et al. 2007). In such situations, HCO$^+$ may be a better tracer of dense gas as it can outshine HCN(1–0) by factors of a few (e.g., Anderson et al. 2014). Since dwarf galaxies are the most plentiful galaxies by number in the universe, and thought to be the "building blocks" for hierarchical galaxy assembly, probing their dense gas will be important for understanding how galaxies assemble their stellar mass. ALMA with Band 2 will be sufficiently sensitive to probe the dense-gas content of such galaxies up to $z \lesssim 0.4$.

3.1.4 Molecular outflows and AGN feedback

Since the seminal discovery that active-galactic nuclei (AGN) can drive powerful outflows that effectively quench star formation (e.g., Di Matteo et al. 2005), AGN feedback has become a cornerstone of galaxy evolution. The most effective mode of studying AGN feedback is arguably through the molecular component of the ISM (e.g., Feruglio et al. 2010; Aalto et al. 2012; Cicone et al. 2012, 2014; Combes et al. 2013, 2014; Garcia-Burillo et al. 2014). The massive molecular outflow in the ULIRG, Mrk 231, the best-studied case so far, has been detected not only in low-J CO transitions (Feruglio et al. 2010; Cicone et al. 2012), but also with high-density tracers including HCN(1–0), HCO$^+$, and HNC (1–0) (Aalto et al. 2012). Moreover, the high-velocity wings that characterize the outflow are more prominent in the higher density gas (traced by HCN) than in the low-J CO lines (Cicone et al. 2012). The implication is that not only very dense ($n_{H2} \gtrsim 10^4$ cm^{-3}) molecules survive in the outflow, but also that the high dipole moment molecules may be enhanced in the wind, and may thus offer the best probe of the energetics of the outflow.

A possible explanation for such enhanced HCN emission in the massive molecular wind can be the presence of strong shocks. While in Mrk 231 the hypothesis of strong shocks is inconsistent with the CO excitation in the outflowing gas (Cicone et al. 2012), in NGC 6240, another ULIRG, there is evidence for shocked gas at the confines of the outflow (Feruglio et al. 2013). Moreover, in addition to negative AGN feedback which quenches star formation, in some cases star formation may be enhanced by the compression of the gas(e.g., Zinn et al. 2013; Cresci et al. 2015). Because of the increased redshift range for tracers of dense-gas outflows, ALMA Band 2+3 will provide a key diagnostic into the physical processes behind feedback in galaxies, exactly over the crucial redshift range where the cosmic SFRD is declining.

Other important molecular transitions can also be observed in galaxies up to $z \sim 0.4$ within

Band 2(or 2+3), including CS (2–1) (97.98 GHz) and SiO (2–1) (86.85 GHz). CS, being particularly resistant to shocks and UV photo-dissociation, is a very good and unbiased tracer of dense molecular gas, and can be used to determine the amount of dense gas in the outflows and its relation with the diffuse component. Silicon monoxide (SiO) is an unambiguous tracer of strong shocks which can modify the chemistry of the local ISM; by destroying dust grains and injecting silicon and SiO into the gas phase, the SiO abundance is enhanced. This molecule represents an independent tool to test the presence of shocks and their relevance in the feedback process. The (1–0) transition of CS and SiO are covered by the ALMA Band 1 and the Q Band of JVLA, but the (2–1) transitions are *crucial to study the excitation of these species* in the outflow. These transitions could also open a new diagnostic for galactic-scale outflows, given that similar physics seem to be driving bipolar outflows from stellar-sized accretion disks (e.g., Sánchez-Monge et al. 2013). ALMA Band 2+3 will open a new window on the physical conditions behind dense gas tracers in galaxies.

3.2   The radio-loud AGN duty cycle: the role of cold gas

Early-type galaxies (ETGs) host a wide range of kinematic sub-structures (e.g. Emsellem et al. 2004), with decoupled prograde stellar disks in the preferentially low-mass fast-rotating galaxies and kinematically-misaligned cores in the preferentially massive slow-rotating spheroids (Emsellem et al. 2011). Why star formation is suppressed in ETGs and how sub-structures form are both hotly debated issues. The solutions to both problems may well be connected. On the one hand, active galactic nucleus (AGN) feedback through radio jets (*jet mode*; Heckman & Best 2014) and radiation from the accretion disk (*radiative mode*) are both thought to to be essential to the suppression of star formation (see Fabian 2012 for a review). On the other hand, the interstellar gas which accretes onto the supermassive black hole (SMBH) and powers the AGN may also form decoupled stellar components, in a manner depending on its mass, origin, and ability (or not) to turn into stars. The SAURON and ATLAS[3D] optical integral-field spectroscopic (IFS) surveys and associated CO follow-ups have clearly demonstrated a causal link between the two in radio-quiet ETGs (e.g. Crocker et al. 2008, 2009, 2011). How feedback loops can be established and sustained over many orders of magnitude in spatial scale, and how the gas migrates from kpc scales to the vicinity of the SMBH, have yet to be understood.

3.2.1   AGN fueling: the role of cold gas

It is generally accepted (Heckman & Best 2014) that radiatively efficient, high-excitation (typically powerful) radio galaxies (HERGs) are triggered by cold gas transported to the centre through merging or collisions with gas-rich galaxies. Allen et al. (2006) however suggested that accretion in radiatively inefficient, low-excitation (typically low-power) radio galaxies (LERGs), that dominate in the local Universe, may occur directly from the hot phase of the intergalactic medium. However, radio galaxies (RGs) of all powers have complex, multi-phase interstellar media, with cold (molecular), cool (HI), warm (ionised) and hot (X-ray) components. LERGs often possess large amounts of dust and molecular gas (e.g. de Koff et al. 2000; Prandoni et al. 2007, 2010; Ocana Flaquer et al. 2010), providing compelling evidence that cold gas could also be the fuel supply. In fact, larger reservoirs of molecular gas are present in LERGs than in radio-quiet galaxies (Senatore et al. 2015).

Several of the LERGs detected in CO have double-horned line profiles (Prandoni et al. 2010; Senatore et al. 2015), consistent with ordered rotation, while HST observations show that dust in these objects is often confined to disks on small (kpc or sub-kpc) scales. The presence of nuclear disks of molecular gas (and dust) may therefore be a common feature in these objects. This is indirectly supported by the systematic CO (1–0) line imaging campaign of a large sample of gas-rich but generally radio-quiet ETGs from ATLAS[3D] (Alatalo et al. 2013), where kpc-scale
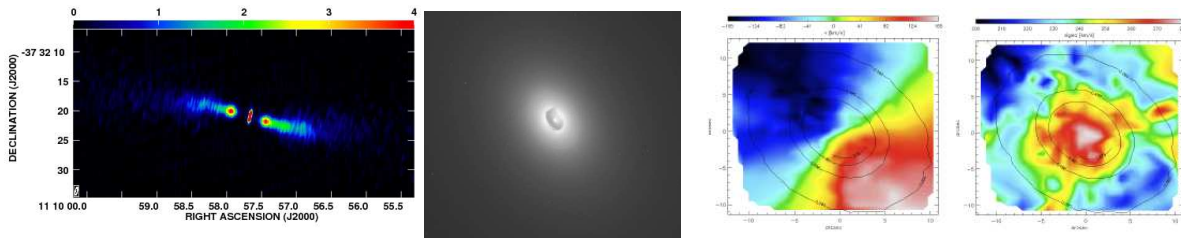
Figure 18: *Observations of NGC 3557.* **Extreme-left:** *5 GHz VLA radio continuum image, showing the inner part of the radio galaxy ($60'' \times 30''$).* **Centre-left:** *HST image of the central regions, revealing a regular nuclear dust disk (Lauer et al. 2005).* **Centre-right:** *VLT/VIMOS IFS mean stellar velocity map of the central regions ($27'' \times 27''$) with overlaid isophotes, revealing ordered rotation.* **Extreme-right:** *Associated stellar velocity dispersion map.*

molecular gas disks were found in 50% of the targets and tend to follow the dust. A regular disk morphology is preferentially associated with more massive ellipticals, the typical hosts of RGs. Nuclear disks may thus be an essential link in the feeding/feedback cycle. One possible scenario is that the CO traces the outer parts of a thin disk that becomes progressively hotter and then ionised at smaller radii. The molecular emission would then have an inner edge, that should be seen at high resolution. It is likely that most of the cold gas in LERGs is in stable orbits (as suggested by Okuda et al. 2005 for the proto-typical LERG 3C 31) and that the black holes are "drip-fed" by molecular clouds from the inner disk. Whether the cold gas in LERGs originates externally (accretion, mergers) or internally (stellar mass loss, cooling of an initially hot gas phase) remains an open question. Comparing the kinematics of the molecular and ionised gas with that of the stars can differentiate between these alternatives (see Davis et al. 2011, 2013a).

3.2.2 Jet-induced Feedback

Radio jets can transport energy efficiently to large distances, they couple efficiently to the interstellar medium (ISM), and they produce fast outflows emanating from the central regions (as required from feedback models; Wagner, Bicknell & Umemura 2012). Several outflows are known to be driven by low-power radio jets, including cases of massive neutral and molecular outflows (e.g. Alatalo et al. 2011; Combes et al. 2013; Morganti et al. 2013; Santoro et al. 2015). This suggests that even jets with low kinetic power can drive outflows, and that the jet-ISM interaction may be a relatively common phenomenon associated with the active phase of a galaxy. It is however surprising that despite the violent interaction, these off-nuclear outflows still have a component of relatively cold gas (< 1000 K), as detected in HI and CO (see also discussion in previous section). One possibility is that the radio jet interacts with the gas close to the nucleus and decelerates from relativistic speeds on kpc scales (Laing & Bridle 2002), entraining some of the denser surrounding material along with it. However, whether this is a common property remains an open question. To probe the above scenarios, we need sub-kpc/kpc imaging of CO or other molecular lines, but only a few of the most spectacular examples have been studied in detail so far. Understanding the incidence, characteristics, and effects of such interactions in a broader statistical manner is crucial to assess the role of jet-induced feedback in galaxy evolution, as well as the jet-ISM interaction physics.

3.2.3 Justification for ALMA Band 2+3

A systematic study of the various gas phases (ionised and molecular) and of the stellar and dust components in the cores of representative samples of massive, radio-loud ETGs (in which jets

are currently active) would enable a better understanding of the feeding of AGNs, and would isolate the role played by jet-induced feedback in the overall formation and evolution of ETGs.

Exploratory studies in the local Universe ($z < 0.03$) are ongoing with VLT-VIMOS (eg. Prandoni et al. 2010; Senatore et al. 2015, see Fig. 18) with the aim of identifying kinematical signatures of feeding/feedback loops that can be causally related to the presence of radio jets. For such studies ALMA can play a crucial role, by imaging the cold (molecular) gas component in CO on kpc and sub-kpc scales, using Bands 3 and 6 to probe the CO (1–0) and (2–1) transitions respectively. The ATLAS^{3D} IFS survey (Cappellari et al. 2011), for which molecular-line imaging is available (Alatalo et al. 2013) provides an excellent control sample of predominantly radio-quietETGs.

With the advent of new-generation integral-field spectrometres, spatially-resolved kinematic studies of the stellar and ionized gas galaxy components can be pushed to significantly higher redshifts. For instance the second-generation *VLT Multi Unit Spectroscopic Explorer (MUSE)* in *Narrow Field Mode* allows to image galaxies on < 300 pc scales at $z < 0.7$. This will allow to identify possible trends with galaxy evolution, using $z \sim 0$ samples as a local Universe constraint. The combination of ALMA Band 2+3 would nicely complement MUSE, allowing to image the CO (1–0) molecular gas components in galaxies on comparable scales up to similar redshifts. Millimeter-VLBI, including ALMA will allow to probe the innermost regions, down to pc scales (see Sect. 3.4 for more details).

3.3 Evolutionary history of galaxy environments

Galaxies occur in a range of environments, from close-pairs to clusters which are the largest collapsed structures in the Universe with total masses up to $10^{15} M_\odot$ (e.g., Arnaud et al. 2009). One of the most important issues is the spatial and temporal evolution of star formation activity within these environments. A key requirement for star formation is the presence of a reservoir of dense, cold gas that can be efficiently converted into stars. This is especially crucial for galaxies in rich clusters, because they are expected to be a affected by mechanisms able to remove cold gas from the haloes and disks of infalling galaxies (e.g., ram pressure stripping, Gunn & Gott 1972) or to prevent further cooling of gas within galaxies' dark matter haloes (starvation or strangulation, e.g., Larson et al. 1980; Bekki et al. 2002). This environmental dependence profoundly influences the evolutionary histories of galaxy clusters and the star formation-galaxy density relation represents a well-established observational hallmark of how galaxies evolve as a function of environment (e.g., Geach et al. 2009).

Studies of star formation activity based on multi-wavelength tracers have shown a gradual truncation, from $z = 0$ to $z \sim 1$, in the cores of rich clusters (e.g., Hashimoto et al. 1998; Ellingson et al. 2001; Gómez et al. 2003; Patel et al. 2009). Determining the nature and modes of star formation requires a robust understanding of the relationship between the gas content of a galaxy and its star formation rate. Remarkable progress has been made in understanding the conversion mechanisms in field galaxies (e.g., Wong & Blitz 2002; Bigiel et al. 2008; Daddi et al. 2010; Genzel et al. 2010; Tacconi et al. 2010; Combes et al. 2011; Casasola et al. 2015), but the cold and dense gas fueling the star formation has been difficult to investigate in clusters (e.g., Wagg et al. 2012), despite their exceptional opportunities for cosmological studies.

We detected, for the first time, CO (2–1) emission with IRAM PdBI in AGN.1317, a source belonging to the galaxy cluster associated with the radio galaxy 7C 1756+6520 at $z \sim 1.4$ and located nearby the centre of the cluster (see Fig. 19). Such CO detections in high-z clusters are rare. From the CO (2–1) line luminosity, we measured H$_2$ mass of $1.1 \times 10^{10} M_\odot$, comparable to that in massive sub-millimeter galaxies. The optical images of the cluster show that AGN.1317 is an isolated object, and thus its gas mass might be an intrinsic characteristic associated with its early evolutionary phase, when most of its baryonic mass was in gas phase, than due to a merger
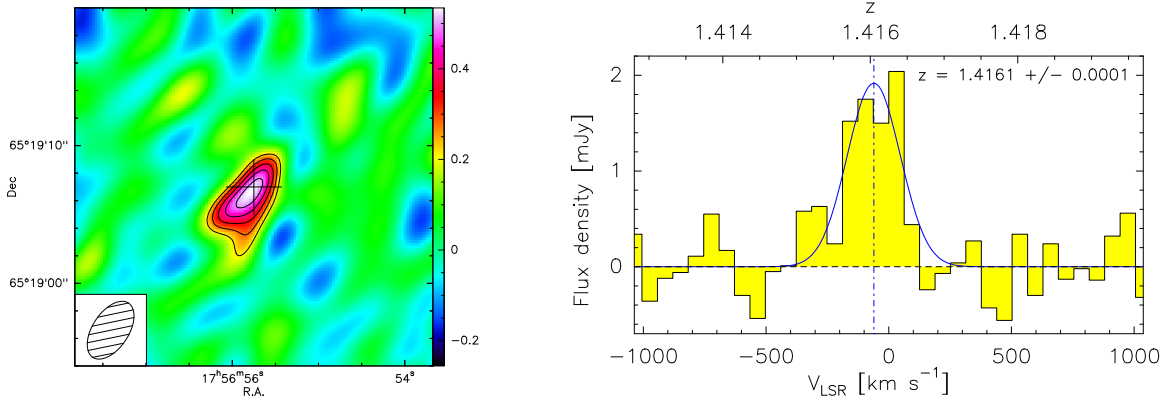
Figure 19: *Left Panel:* CO (2–1) intensity map obtained with the IRAM PdBI toward AGN.1317. The color wedge of the intensity map is in Jy beam^{-1} km s^{-1}. The black cross marks the coordinates of the phase tracking centre of observations. The *rms* noise level is $\sigma = 0.07$ Jy beam^{-1} km s^{-1} and contour levels run from 3σ to 7σ with 1σ spacing. In this map a velocity range of $\sim$360 km s^{-1} is used. The beam of $4.73'' \times 2.33''$ (PA = 147°) is plotted at lower left. *Right Panel:* CO (2–1) integrated spectrum obtained with the IRAM PdBI toward AGN.1317 centred on the optical velocity of AGN.1317, $V_{opt} = 4.25 \times 10^5$ km s^{-1} ($z = 1.4162$, Galametz et al. 2010) Figures from Casasola et al. (2013).

episode with nearby companions. The Hα-derived star formation rate (SFR) is $\sim 65\, M_\odot$ yr^{-1}, and so AGN.1317 would exhaust its reservoir of cold gas in $\sim$0.2–1.0 Gyr. This relatively high molecular gas content and SFR for an AGN near the center of a young cluster is compatible with models of evolution of galaxy clusters that predict high SFR at the epoch of their formation, i.e. $z \sim 1.5$. Following the predictions of those models, at $z \sim 1$, the SFR would rapidly be quenched through environmental effects starting from the innermost regions of clusters. Very recently, we obtained near-infrared observations at the Large Binocular Telescope (LBT) to map the whole AGN population associated with the radio galaxy 7C 1756+6520. We detected Hα, Hβ, [O III], [N II], and Fe II line emissions in four AGN and defined other new eleven sources with redshift consistent with that of the cluster (Fig. 20, Casasola et al. in prep.). Based on these LBT results we are selecting single cluster galaxies for observations of CO (2–1) at the IRAM PdBI and of CO (1–0) at the JVLA and to deeply investigate the nature and modes of star formation in this primordial cluster.

So far, cold gas has been detected in cluster galaxies only up to $z \sim 0.5$, especially in the outskirts of rich clusters (e.g., Geach et al. 2009; Jablonka et al. 2013), while the range $z \sim 0.5 - 1$ is yet unexplored. For the first time, ALMA Band 2 will offer the opportunity to study the CO (1–0) line in group and cluster galaxies at $z \sim 0.3 - 0.7$, in a redshift range where the gas-star conversion in clusters is completely unexplored. Although similar redshift ranges are observable in other ALMA bands (i.e., Band 6 for CO (3–2) and Band 4 for CO (2–1)), Band 2 enables accurate estimates of molecular gas content without ambiguity on the H$_2$–CO conversion factor. In addition, Band 2 offers a field-of-view $\sim$2–3 times larger (depending on the redshift range) than other ALMA bands at higher frequencies; clusters at $z > 1$ are generally $< 1'$ in size (e.g., Wagg et al. 2012; Casasola et al. 2013) so that the Band 2 field-of-view of $70 - 90''$ gives coverage of the entire cluster and resolves individual cluster members with only a single pointing. Observations of cluster members covering a wider radial range can help distinguish the various physical processes expected to play a role (e.g., ram-pressure stripping, strangulation, tidal interactions, and mergers) because these processes peak in effectiveness at different clustercentric radii (Moran et al. 2007; De Lucia et al. 2010). How, when, and where
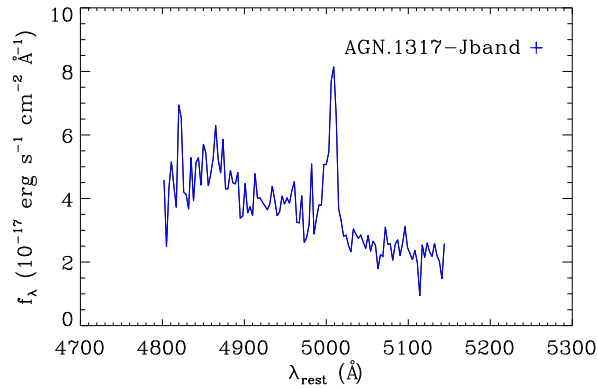
Figure 20: *J-band spectrum obtained with the LBT toward AGN.1317. It shows the detection of* [O III] *at 5700 Å and Hβ at 4861 Å. Figure from Casasola et al. (in preparation).*

such mechanisms affect the evolution of galaxies has yet to be explored.

3.4   Observations of deuterated molecules in nearby galaxies

In the 40 years since the first molecular detection in the extragalactic interstellar medium, the number of species identified in external galaxies is now more than 50.

Many of these species have been observed in nearby starburst galaxies, an obvious target of mm/submm spectral surveys (Martin et al. 2006, 2011; Aladro et al. 2011, 2012; Requena-Torres et al. 2011), due to their molecular brightness.
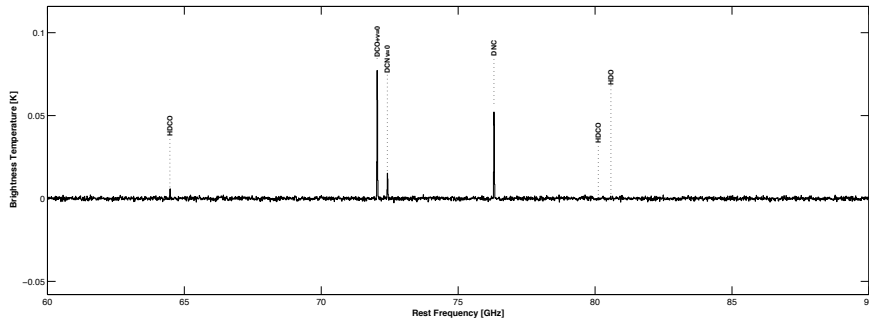

Figure 21: *The simulation is based on a on time of 6h; rms 0.00072 K; resolution 4"; full ALMA freq: 90 GHz; Spectral resolution 50 km/s; Line width=100 km/s; $N(H_2)=1\times10^{23}$ cm^{-2}; $N(Deut.\ Mol)=1\times10^{13}$ cm^{-2}; $T_k=10$ K*

ALMA's sensitivity will certainly increase the number of detections in "normal" starforming galaxies, so far mainly observed in the two most abundant molecules, tracing star formation: CO and HCN. The study of chemical composition and physics of the interstellar gas in star-forming regions is extremely important in order to understand the complex processes of star formation. Observations of molecular lines of many species provide comparative molecular abundances and inferences on the evolution of physical conditions and atomic abundances in galaxies. CO is widely used to map the distribution of molecular hydrogen, but in dense star forming regions it can be highly depleted or photodissociated: in these cases observations of other molecular tracers become extremely important. In highly embedded star forming regions, where CO is

34

depleted, the chemistry is driven by deuterated species. In our Galaxy, in such regions, a large deuterium fractionation is observed, well above the elemental abundance ratio D/H of 1.5×10^{-5}. Deuteration in extragalactic star-forming environments, where the physical conditions can be drastically different from what we see in our own Galaxy, is almost an unexplored territory. Observations of deuterated molecules in external galaxies will help determining (i) the D/H ratio, which depends on the degree of processing of the gas, and hence can give us clue on the evolution of the gas in a galaxy as well as be used as tracer of nucleosynthesis in the Big Bang, and (ii) the depletion in dense gas in external galaxies which will give us clues on the star formation process.

3.4.1 Justification for ALMA Band 2+3

ALMA Band 2 will make accessible a range of frequencies where no interferometric capabilities currently exist. Some deuterated molecular transitions are uniquely observable in ALMA Band 2, such as: DCO^+ (1–0), DCN (1–0), DNC (1–0), N_2D^+ (1–0). Astrochemical models (Bayet et al. 2010) have explored a large parameter space of physical conditions covering different extragalactic environments and provided a guide to observations of deuterated molecules arising from the dense gas in external galaxies. Although qualitative in nature, the models led to some important conclusions: (i) HDO and DCN are abundant, regardless of the extragalactic environment; and (ii) DCO^+ is a tracer of cosmic rays enhanced gas. Clearly, observations of the fundamental transitions, in Band 2 give the best chance of optimizing the detection of these species. A tentative detection of DCN (2–1) line has been reported by Martin et al. (2006) in the nucleus of NGC253. This detection, if confirmed, would be in agreement with the prediction of a cosmic ray enhanced environment in that region. NGC253 would be the ideal target for an observational campaigns aiming at validating the model predictions. Figure 21 shows an example of a simulated ALMA spectrum in Band 2 containing the selected deuterated species.

3.5 Imaging super-massive black holes and origin of AGN jets with mm-VLBI

3.5.1 mm-VLBI with ALMA

The huge potential of Very Long Interferometer (VLBI) technique at submm/mm wavelengths is that it enables the highest resolution imaging currently possible at any wavelength in astronomy, achieving about 20 microarcsecs for a 9000 km baseline at 1.3 mm. The use of ALMA as a phased array to form part of a global VLBI network will offer unprecedented sensitivity at very high angular resolution, making one order of magnitude weaker sources accessible to μas-resolution studies and greatly improving image fidelity for the brighter objects (Fish et al. 2013, Tilanus et al. 2014) . Existing activities at 3 mm (the Very Long Baseline Array and the Global Millimeter VLBI Array) and at 1 mm (the Event Horizon Telescope project) have laid the ground work for future coordinated observations. An international consortium is presently constructing a beamformer for the ALMA that will be available as a facility instrument providing substantial improvements to existing VLBI arrays at 7 and 3 mm. The wide mm-VLBI science achievable by a beamformer for ALMA has recently been discussed by Fish et al. (2013) and Tilanus et al. (2014). In the following, we discuss the AGN science cases that will be possible thanks to ALMA Band 2 or Band 2+3 observations in conjunction with other millimetre telescopes.

3.5.2 Event horizon scale imaging

The inclusion of the phased ALMA in global mm-VLBI observations will open new frontiers, offering the very high sensitivity and high angular resolution necessary to image the emission around nearby super massive black holes, even on event horizon scales. This will provide tests

not only of the black hole paradigm, Einstein's General Theory of Relativity (GR) in its strong-field limit, but also of e.g., the "cosmic censorship" conjecture and the "no-hair" theorem (Fish et al. 2013, Tilanus et al. 2014). Because of their vicinity, the principal targets for this kind of analysis are SgrA* and M87. Each mm-VLBI frequency penetrates a different depth into the black hole environment. Full frequency coverage, including Band 2 or 2+3, is needed to distinguish between changes in spectral index due to scattering or due to intrinsic changes in emitting material and relativistic effects. While for SgrA* the scattering in Band 2 could be a critical issue, for M87, which is actively accreting material and emitting jets on kilo-parsec scale, Band 2 or 2+3 observations would probe (European Science Case for ALMA Band 2: Fuller et al., in preparation) the material at around 12 Schwarzschild radii where the spectral energy distribution (SED) deviates from a power law and variability is increasingly rapidly (Hada et al. 2012).

3.5.3 Jet launching region study

As well explained in Fish et al. (2013) and Tilanus et al. (2014), the mm-VLBI is also the only method to directly image the AGN jets down to their formation region and study the acceleration/collimation zone in the optically thin regime, i.e. on Schwarzschild radius scales where magneto-hydrodynamic (MHD) instabilities form. The very high sensitivity feasible thanks to the inclusion of the phased ALMA in mm-VLBI observations will provide a great chance to explore for the first time these jet regions in fainter AGN. Intriguing targets (see Tilanus et al. 2014) are for example the LLAGN, where cm-wavelength VLBI has already provided interesting clues; blazars, where the high-energy emission sites and mechanisms are uncertain; and sources with double-sided jets for which mm-VLBI observations can provide a direct determination of the location of the central engine relative to the jet and counter-jet features. Band 2 VLBI could provide an ideal balance of resolution and flux density necessary to investigate the launching jet region in these nearby (week) AGN. This is the case of the compact active galaxies studied by Liuzzo et al. 2013 with observed small-scale nucleus radio structures posing questions such as the origins of FRI and the evolution of BL Lac objects but with SEDs suggesting significant features in the frequency range covered by Band 2 or 2+3.

3.5.4 Jet polarization analysis

Not only the mm-VLBI continuum analysis will be essential but also the polarization study is fundamental in the understanding of the jet launching mechanisms. Polarimetry with mm-VLBI is indeed a unique tool to image at Schwarzchild radii the intrinsic magnetic field configuration, helping to discriminate whether the jets are launched by MHD effects (Tilanus et al. 2014). Observations of changes in jet position angle with frequency could reveal a helical nature, or time-change in orientation of the mm-wavelength jet could be related to precession of the relativistic jet. Good frequency coverage, including Band 2 or 2+3, is therefore essential (European Science Case for ALMA Band 2: Fuller et al., in preparation) to trace the spectral curvature, identify the jet flaring region and avoid ambiguities in Faraday rotation analysis due to the polarization angle changing very rapidly with frequency (Porth et al. 2011). Recently, it has been also suggested that the Band 2 or 2+3 emitting region is complex, with a three-dimensional structure. The possible comparison of Band 2 or 2+3 polarimetric observations with space-VLBI (e.g., RADIOASTRON) ones at 22 GHz will allow to trace the 3D-field with an angular resolutions better than 50 microarcseconds and to determine the Rotation Measure (Tilanus et al. 2014).

Finally, mm-VLBI polarimetric observations could trace (European Science Case for ALMA Band 2: Fuller et al., in preparation) the evolution of the magnetic field after flares in blazars and give important hints on the origin of their high energy emission (e.g., Orienti et al. 2013). For example, the possible change of the mm-VLBI polarization properties close in time with

some high energy flares could be related either to the propagation of a shock along the jet that orders the magnetic field, or a change of the opacity regime.

3.6 ALMA Band 2 Science case: The Sunyaev-Zel'dovich effect

3.6.1 Sunyaev-Zel'dovich effect in Galaxy clusters

The Sunyaev-Zel'dovich effect (SZE) is the spectral distortion of the Cosmic Microwave Background (CMB) due to inverse Compton scattering of CMB photons off a cloud of electrons (Birkinshaw 1999; Carlstrom et al. 2002). The increase of the photon energy implies a decrease of the CMB brightness at frequencies below 218 GHz and an increase at higher frequencies. The minimum of the CMB brightness (i.e., the maximum of the distortion) is reached at about 128 GHz. The amplitude of the distortion depends only on the properties of the electron cloud: in the case of thermal electrons it is proportional to the integral of the electron pressure (i.e. $T_{SZ} \propto T_e n_e$, where n_e is the electron density and T_e is the electron temperature) along the line of sight, and is independent of distance.

Galaxy clusters are massive structures permeated by hot dense ionized gas that preserves the same cosmic baryonic fraction of the epoch of the cluster virialization, so they are the ideal targets for SZE observations and to infer pieces of information about cosmology. The absolute X-ray luminosity from the hot cluster gas has a different dependence on gas properties and is dependent on the cluster redshift. For virialized clusters, where the distribution of density and temperature are easy to model with regular forms (e.g., isothermal and spherically symmetric), the different distance dependence provides a powerful method to extract cosmological parameters by combining the two signals. The comparison of the two signals is also a particularly effective tool to estimate the gas mass but the different dependence on density makes X-ray more susceptible to the gas clumping. The SZE signal is a better tracer of less dense hotter region.

Current theories of structure formation predict that clusters form hierarchically via merger of smaller structures (Borgani et al. 2001). X-ray observations (Jeltema et al. 2005; Maughan et al. 2008) of high redshift ($z > 0.5$) clusters revealed that they are more morphologically complex, less virialized and dynamically more active than low-redshift clusters. Studies of $z > 0.8$ clusters show clumpy and elongated structures suggesting that they are close to the epoch of cluster formation (Rosati et al. 2004). The study of high redshift cluster SZE can provide constraints on the theories of cluster formation and evolution. However,for these objects the temperature and density distributions might be so complex that the comparison of X-ray and SZE signals is seriously compromised, and the information about cosmology or cluster evolution will be misleading. Sub-arcmin resolution centimetric wavelength observations with ATCA and EVLA (Massardi et al. 2010; Malu et al. 2010; Mason et al. 2010) of 3 $z > 0.8$ clusters (Cl0152-1357, the Bullet cluster and Cl 1357-1145 respectively) confirmed that the structure are morphologically complex and that there is a displacement of the peak of SZ with respect to the X-ray emission peak, most likely under the effect of merging events, and strongly indicating the need for sub arcmin resolution observations to properly compare the signals and characterize the cluster structure if far from virialization. These conclusions were confirmed by single dish observations at 90 GHz (Korngut et al. 2011).

Furthermore, by combining X-ray emission with sub-arcmin scale SZE can probe turbolence and entropy excesses investigating the intra-cluster medium (ICM) pressure fluctuations, the dynamics of shocks and blasts that enhance the SZ signal within the ICM, the temperature and density profile of the ICM. This will also help to understand the cooling flows mechanisms and the AGN feedback within the ICM. Finally, ALMA will be crucial to follow-up of galaxy clusters detected in large area surveys (e.g. PCSZ, Planck Collaboration et al. 2014)

Justification for ALMA Band 2+3   The SZE signal is also typically contaminated by radio source emission which is usually associated to early-type galaxies which preferentially reside in galaxy clusters. In mm bands, the radio component decreases and the contribution due to dust emission from star-forming galaxies in the cluster increases with frequency. The minimum of the contribution is in the so-called "cosmological window" at about 70 GHz. Observations in band 2+3 earn in resolution with respect to centimetric observations so far available without losing in sensitivity as the absolute value of the SZE increase by almost an order of magnitude. Point sources can be also directly observed (and removed on the uv plane) by exploiting the longer baselines of the main ALMA array, and the overall SZ signal can be measured by mean of the total power antennas.

3.6.2   Sunyaev-Zel'dovich in early stages of galaxy formation

Since SZ is independent of distance it is a powerful tool of investigation of high redshift structures permeated by hot electron clouds like galaxy clusters and star forming galaxies. In the standard galaxy formation scenario plasma clouds with a high thermal energy content must exist at high redshifts since the protogalactic gas is shock heated to the virial temperature, and extensive cooling, leading to efficient star formation, must await the collapse of massive haloes (downsizing, see Granato et al. 2004; Massardi et al. 2008). Model of emission from the early stages of galaxy formation pointed out that thermal SZE from the virializing gas is their most significant signal of emission in the radio-mm band. The signal is of the order of 1 μK at 3–4 mm wavelength on 10 arcsec angular scales

Justification for ALMA Band 2+3   Model-based estimations indicate that we will need about 30 h on source to survey 1sqdeg down to about 10^{-4} Jy, where we can detect up to 100 proto-galaxies with ALMA Band 2+3 (70–100 GHz). Band 2 should be preferred for the lower level of dust contamination. Radio luminosity from star formation in the core regions steeply increases with frequency. Thermal dust emission from the core region increases with frequency and overwhelms SZ signal at 100 GHz. In the range 35–80 GHz observations of thermal SZ is possible for most massive haloes. Arcsec resolution images may reconstruct the uncontaminated SZ signal by distinguishing contaminating emissions on the scale of the stellar distributions (<1 arcsec at $z > 1$) and the SZ effects on the scale of the dark matter halo (typically ten times larger) and by detecting and subtracting out the confusion effect by radio sources.

References

Aalto, S., Booth, R. S., Black, J. H., & Johansson, L. E. B. 1995, A&A, 300, 369
Aalto, S., Garcia-Burillo, S., Muller, S., et al. 2012, A&A, 537, AA44
Aladro, R. et al., 2011, A&A, 535A, 84A
Aladro, R. et al., 2012, A&A, 549A, 39A
Alatalo, K., Blitz, L., Young, L.M., et al. 2011, ApJ, 735, 88
Alatalo, K., Davis, T.A., Bureau, M., et al. 2013, MNRAS, 432, 1796
Allen, S. W., Dunn, R. J. H., Fabian, A. C., Taylor, G. B., Reynolds, C. S. 2006, MNRAS, 372, 21
Anderson, C. N., Meier, D. S., Ott, J., et al. 2014, ApJ, 793, 37
Aravena, M., Carilli, C., Daddi, E., et al. 2010, ApJ, 718, 177
Arce, H.G., Santiago-García, J., Jörgensen, J.K., Tafalla, M., Bachiller, R. 2008, A&A 681, L21
Armijos-Abendaño, J., Martín-Pintado, J., Requena-Torres, M. A., et al. 2015, MNRAS, 446, 3842
Arnaud, M. 2009, A&A, 500, 103
Arzner K., Güdel M., Briggs K., Telleschi A., Audard M., 2007, A&A, 468, 477
Bachiller, R., Pérez Gutiérrez, M., Kumar, M.S.N., Tafalla, M. 2001, A&A 372, 899
Bacmann, A., Taquet, V., Faure, A., Kahane, C., Ceccarelli, C. 2012, A&A 541, L12
Bartkiewicz A., Szymczak M., van Langevelde H. J., et al. 2009, A&A, 502, 155

Bayet, E. et al., 2010, ApJ, 725, 214

Bekki, K., Couch, W. J., & Shioya, Y. 2002, ApJ, 577, 651

Beltrán, M. T., Codella, C., Viti, S., Neri R., Cesaroni, R. 2009, A&A, 690, L93

Beltrán M. T., Sánchez-Monge Á., Cesaroni R., et al. 2014, A&A, 571, A52

Benedettini, M., Viti, S., Codella, C., et al. 2013, MNRAS 436, 179

Bergin, E. A., Aikawa, Y., Blake, G. A., & van Dishoeck, E. F. 2007, Protostars and Planets V, 751

Bergin, E. A., Cleeves, L. I., Gorti, U., et al. 2013, Nature, 493, 644

Bigiel, F., Leroy, A., Walter, F., et al. 2008, AJ, 136, 2846

Birkinshaw, M. 1999, Physics Reports, 310, 97

Bisschop, S.E., Jörgensen, J.K., Bourke, T.L., Bottinelli, S., van Dishoeck, E.F. 2008, A&A 488, 959

Bolatto, A. D., Wolfire, M., & Leroy, A. K. 2013, ARA&A, 51, 207

Bower et al., 2003, ApJ 598, 1140

Borgani, S., & Guzzo, L. 2001, Nature, 409, 39

Bottinelli, S., Ceccarelli, C., Williams, J. P., & Lefloch, B. 2007, A&A, 463, 601

Buchbender, C., Kramer, C., Gonzalez-Garcia, M., et al. 2013, A&A, 549, AA17

Calcutt, H., Viti S., Codella C., Betrán M., Fontani F., 2014, MNRAS, 433, 3157

Cappellari, M., Emsellem, E., Krajnović, D., et al. 2011, MNRAS, 413, 813

Carilli, C. L., & Walter, F. 2013, ARA&A, 51, 105

Carlstrom, J. E., Holder, G. P., & Reese, E. D. 2002, ARA&A, 40, 643

Carr, J. S. & Najita, J. R. 2008, Science, 319, 1504

Casasola, V., Magrini, L., Combes, F., et al. 2013, A&A, 558, A60

Casasola, V., Hunt, L., Combes, F., & Garcia-Burillo, S. 2015, A&A, 577, A135

Caselli, P. & Ceccarelli, C. 2012, A&ARv, 20, 56

Caselli, P., Keto, E., Bergin, E.A., et al. 2012, ApJ 759, L37

Cazaux, S., Tielens, A. G. G. M., Ceccarelli, C., et al. 2003, ApJL, 593, L51

Ceccarelli, C., Caselli, P., Herbst, E., Tielens, A.G.G.M., Caux, E. 2007, Protostars and Planets V, University of Arizona Press, Tucson, 47

Cernicharo, J. et al. 2012, ApJ, 759, L43

Cesaroni, R. 2008, Ap&SS, 313, 23

Cesaroni, R., Galli, D., Lodato, G., Walmsley, M., Zhang, Q. 2007, Protostars and Planets V, 197

Cesaroni, R., Hofner, Walmsley, C. M., & Churchwell, E. 1998, A&A, 331, 709

Chapillon, E., Dutrey, A., Guilloteau, S., et al. 2012b, ApJ, 756, 58

Chapillon, E., Guilloteau, S., Dutrey, A., Piétu, V., & Guélin, M. 2012a, A&A, 537, A60

Cicone, C., Feruglio, C., Maiolino, R., et al. 2012, A&A, 543, AA99

Cicone, C., Maiolino, R., Sturm, E., et al. 2014, A&A, 562, AA21

Codella, C., Benedettini, M., Beltrán, M.T., et al. 2009, A&A 507, L25

Codella, C., Fontani, F., Ceccarelli, C., et al. 2015, ApJ 449, L11

Collins, P. & Ferrier, R., 1995, Monosaccharides (New York: Wiley)

Combes, F., García-Burillo, S., Braine, J., et al. 2011, A&A, 528, A124

Combes, F., García-Burillo, S., Casasola, V., et al. 2013, A&A, 558, AA124

Combes, F., García-Burillo, S., Casasola, V., et al. 2014, A&A, 565, AA97 Costagliola, F., Aalto, S., Rodriguez, M. I., et al. 2011, A&A, 528, AA30

Coutens, A., Persson, M. V., Jørgensen, J. K. et al. 2015, A&A, 576, 5

Coutens, A., Vastel, C., Cabrit, S., et al. 2013, A&A, 560, A39

Coutens, A., Vastel, C., Caux, E., et al. 2012, A&A, 539, A132

Cragg D. M., Sobolev A. M., and Godfrey P. D. 2005, MNRAS, 260, 533

Crapsi, A., Caselli, P., Walmsley, C.M., et al. 2005, ApJ, 619, 379

Cresci, G., Mainieri, V., Brusa, M., et al. 2015, ApJ, 799, 82

Crocker, A.F., et al. 2008, MNRAS, 368, 1811

Crocker, A.F., et al. 2009, MNRAS, 393, 1255

Crocker ,A.F., et al. 2011, MNRAS, 410, 1197

Daddi, E., Bournaud, F., Walter, F., et al. 2010, ApJ, 713, 686

Daddi, E., Elbaz, D., Walter, F., et al. 2010, ApJL, 714, L118

Danielson, A. L. R., Swinbank, A. M., Smail, I., et al. 2011, MNRAS, 410, 1687

Dannerbauer, H., Daddi, E., Riechers, D. A., et al. 2009, ApJL, 698, L178

Dauphas, N., Robert, F., & Marty, B. 2000, Icarus, 148, 508

Davis, T.A., Alatalo, K., Sarzi, M., et al. 2011, MNRAS, 417, 882

Davis, T.A., Alatalo, K., Bureau, M., et al. 2013a, MNRAS, 429, 534

Davis, T.A., et al., 2013b, Nature, 494, 328

De Lucia, G., Boylan-Kolchin, M., Benson, A. J., Fontanot, F., & Monaco, P. 2010, MNRAS, 406, 1533

Di Francesco et al., 2008, ApJS, 175, 277

Di Matteo, T., Springel, V., & Hernquist, L. 2005, Nature, 433, 604

Drake S. A., Linsky J. L., 1989, AJ, 98, 1831

Dullemond, C. P., Hollenbach, D., Kamp, I., & D'Alessio, P. 2007, Protostars and Planets V, 555

Dutrey, A., Guilloteau, S., & Guelin, M. 1997, A&A, 317, L5

Dutrey, A., Semenov, D., Chapillon, E., et al. 2014, Protostars and Planets VI, 317

Dutrey, A., Wakelam, V., Boehler, Y., et al. 2011, A&A, 535, A104

Ellingson, E., Lin, H., Yee, H. K. C., & Carlberg, R. G. 2001, ApJ, 547, 609

Elsila, J.E., Glavin, D.P., Dworkin, J.P. 2009, M&PS 44, 1323

Emsellen E., Cappellari, M., Peletier, R.F., et al. 2004, MNRAS, 352, 721

Emsellem, E., Cappellari, M., Krajnović, D., et al. 2011, MNRAS, 414, 888

Fabian, A.C. 2012, ARA&A, 50, 455

Fedoseev, G. et al., 2015, MNRAS, 448, 1288

Feigelson & Montmerle 1999 ARA&A 37, 363

Feruglio, C., Fiore, F., Maiolino, R., et al. 2013, A&A, 549, AA51

Feruglio, C., Maiolino, R., Piconcelli, E., et al. 2010, A&A, 518, LL155

Fish, V., Alef, W., Anderson, J., et al. 2013, arXiv:1309.3519

Fontani, F., Busquet, G., Palau, A., Caselli, P. et al. 2015, A&A, 575, 87

Fontani, F., Codella, C., Ceccarelli, C., Lefloch, B., Viti, S., Benedettini, M. 2014, ApJ 788, L43

Forbrich J., Preibisch T., Menten K. M. et al. 2007, A&A, 464, 1003

Forbrich et al., 2008, A&A, 477, 267

Forbrich & Wolk 2013 A&A 551, 56

Fuente, A, Cernicharo, J., Agúndez, M., et al. 2010, A&A, 524, A19

Fuente, A, Cernicharo, J., Caselli, P., et al., 2014, 568, 65

Fuller, G., et al., in preparation, "The Science Case for ALMA Band 2"

Galametz, A., Stern, D., Stanford, S. A., et al. 2010, A&A, 516, A101

Gao, Y., & Solomon, P. M. 2004, ApJ, 606, 271

García-Burillo, S., Usero, A., Alonso-Herrero, A., et al. 2012, A&A, 539, AA8

García-Burillo, S., Combes, F., Usero, A., et al. 2014, A&A, 567, AA125

Geach, J. E., Smail, I., Coppin, K., et al. 2009, MNRAS, 395, L62

Genzel, R., Tacconi, L. J., Gracia-Carpio, J., et al. 2010, MNRAS, 407, 2091

Genzel, R., Tacconi, L. J., Lutz, D., et al. 2015, ApJ, 800, 20

Gerin, M., Goicoechea, J. R., Pety, J., Hily-Blant, P. 2009, A&A, 494, 977

Getman K. V., Feigelson E. D., Micela G. et al. 2008, ApJ, 688, 437

Glavin, D.P., Dworkin, J.P., Aubrey, A., et al. 2006, M&PS 41, 889

Glover, S. C. O., & Mac Low, M.-M. 2011, MNRAS, 412, 337

Glover, S. C. O., Federrath, C., Mac Low, M.-M., & Klessen, R. S. 2010, MNRAS, 404, 2

Gómez, P. L., Nichol, R. C., Miller, C. J., et al. 2003, ApJ, 584, 210

Granato, G. L., De Zotti, G., Silva, L., Bressan, A., & Danese, L. 2004, ApJ, 600, 580

Güdel 2002 ARA&A 40, 217

Gueth F., Guilloteau S., & Bachiller R. 1996, A&A 307, 891

Gueth F., Guilloteau S., & Bachiller R. 1998, A&A 333, 287

Guilloteau, S., Di Folco, E., Dutrey, A., et al. 2013, A&A, 549, A92

Gunn, J. E., & Gott, J. R., III 1972, ApJ, 176, 1

Hada, K., Kino, M., Nagai, H., et al. 2012, ApJ, 760, 52

Halfen, D. T., Apponi, A. J., Woolf, N., Polt, R.; Ziurys, L. M., 2006, ApJ, 639, 237

Hartogh, P., Lis, D. C., Bockelée-Morvan, D., et al. 2011, Nature, 478, 218

Hashimoto, Y., Oemler, A., Jr., Lin, H., & Tucker, D. L. 1998, ApJ, 499, 589

Heckman, T.M., Best, P.N. 2014, ARAA, 52, 589

Hogerheijde, M. R., Bergin, E. A., Brinch, C., et al. 2011, Science, 334, 338

Hollis, J.M., Lovas, F.J., & Jewell, P.R. 2000, ApJ, 540, L107

Hollis, J. M. et al., 2002, ApJ, 571, 59

Holtom, P.D., Bennett, C.J., Osamura, Y., Mason, N.J., Kaiser, R.I. 2005, ApJ 626, 940

Ivison, R. J., Papadopoulos, P. P., Smail, I., et al. 2011, MNRAS, 412, 1913

Jablonka, P., Combes, F., Rines, K., Finn, R., & Welch, T. 2013, A&A, 557, A103

Jeltema, T. E., Canizares, C. R., Bautz, M. W., & Buote, D. A. 2005, ApJ, 624, 606

Jiménez-Serra, I., Testi, L., Caselli, P., Viti, S. 2014, ApJ 787, L83

Jörgensen, J.K., Favre, C. Bisschop, S.E., Bourke, T.L., van Dishoeck, E.F., Schmalzl, M. 2012, ApJ 757, L4

Jörgensen, J.K., & van Dishoeck, E. F. 2010, ApJL, 725, L172

Juneau, S., Narayanan, D. T., Moustakas, J., et al. 2009, ApJ, 707, 1217

Keto, E. 2002, ApJ, 580, 980

de Koff, S, Best, P, Baum, S. A., et al 2000, ApJS, 129, 33

Korngut P. M., et al., 2011, ApJ, 734, 10

Kuiper R., Klahr H., Beuther H., et al. 2010, ApJ, 722, 1556

Kundu et al., 2000, ApJ 545, 1084

Kurtz, S. 2005, IAUS 227, 111

Lagos, C. D. P., Baugh, C. M., Lacey, C. G., et al. 2011, MNRAS, 418, 1649

Laing, R. A., Bridle, A.H. 2002, MNRAS, 336, 328

Larson, R. B., Tinsley, B. M., & Caldwell, C. N. 1980, ApJ, 237, 692

Lauer, T. R., Faber, S. M., Gebhardt, K., et al. 2005, AJ, 129, 2138

Lee, C.-F., Hirano, N., Zhang, Q., et al. 2014, ApJ, 786, 114

Liu H. B., Galván-Madrid R., Forbrich J. et al. 2014, ApJ, 780, 155

Liuzzo, E., Buttiglione, S., Giovannini, G., et al. 2013, A&A, 550, AA76

López-Sepulcre, A., Mendoza, E., Lefloch, B., et al. 2015, MNRAS, in press

Malu, S. S., Subrahmanyan, R., Wieringa, M., & Narasimha, D. 2010, arXiv:1005.1394

Maret S., Hily-Blant P., Pety J., et al., A&A 526, A47

Martin, S. et al., 2006, ApJS, 164, 450

Martin, S. et al., 2011, IAUS, 280, 351

Mason, B. S., Dicker, S.,Korngut, P., et al. 2010, Bulletin of the American Astronomical Society, 42, #364.06

Massardi, M., Ekers, R. D., Ellis, S. C., & Maughan, B. 2010, ApJL, 718, L23

Massi et al., 2006, A&A, 453, 959

Mathews, G. S., Klaassen, P. D., Juhász, A., et al.
2013, A&A, 557, A132

Matsui, T. & Abe, Y. 1986, Nature, 322, 526

Maughan, B. J., Jones, C., Forman, W., & Van Speybroeck, L. 2008, ApJS, 174, 117

Maury, A. J., et al., 2014, A&A, 563, 2

Meijerink, R., Spaans, M., & Israel, F. P. 2007, A&A, 461, 793

Mendoza, E., Lefloch, B., López-Sepulcre, A., et al. 2014, MNRAS 445, 151

Menten K. M. 1991, ApJ, 380, L75

Minier V., Ellingsen S. P., Norris R. P., et al. 2003, A&A, 403, 1095

Modica, P. & Palumbo, M. E. 2010, A&A, 519, A22

Moran, S. M., Ellis, R. S., Treu, T., et al. 2007, ApJ, 671, 1503

Morbidelli, A., Chambers, J., Lunine, J. I., et al. 2000, Meteoritics and Planetary Science, 35, 13

Morganti, R., et al. 2013, Science, 341, 1082

Moscadelli L., Cesaroni R., Rioja M. J., et al. 2011, A&A. 526, A66

Mumma, M. J. & Charnley, S. B. 2011, ARA&A, 49, 471

Muñoz Caro, G. M., Meierhenrich, U. J., Schutte, W. A., et al. 2002, Nature, 416, 403

Narayanan, D., Cox, T. J., Hayward, C. C., Younger, J. D., & Hernquist, L. 2009, MNRAS, 400, 1919

Narayanan, D., Krumholz, M. R., Ostriker, E. C., & Hernquist, L. 2012, MNRAS, 421, 3127

Neufeld, D.A., Nisini, B., Giannini, T., et al. 2009, ApJ 706, 170

Öberg, K. I., Guzmán, V. V., Furuya, K., et al. 2015, Nature, 520, 198

Öberg, K. I., Qi, C., Fogel, J. K. J., et al. 2010, ApJ, 720, 480

Öberg, K. I., Qi, C., Fogel, J. K. J., et al. 2011, ApJ, 734, 98

Ocaña Flaquer, B., Leon, S., Combes, F., & Lim, J. 2010, A&A, 518, A9

Okuda, T., Kohno, K., Iguchi, S., & Nakanishi, K. 2005, ApJ, 620, 673

Orienti, M., Koyama, S., D'Ammando, F., et al. 2013, MNRAS, 428, 2418

Palla F., Stahler S. W., 1993, ApJ, 418, 414

Patel, S. G., Holden, B. P., Kelson, D. D., Illingworth, G. D., & Franx, M. 2009, ApJL, 705, L67

Persson, M. V., Jørgensen, J. K., van Dishoeck, E. F., & Harsono, D. 2014, A&A, 563, A74

Pizzarello, S., Krishnamurthy, R. V., Epstein, S., & Cronin, J. R. 1991, GeCoA, 55, 905

Planck Collaboration, et al., 2014, A&A, 571, A29

Podio, L., Codella, C., Gueth, F., et al. 2015, A&A, in press, arXiv:1505.05919

Podio, L., Kamp, I., Codella, C., et al. 2013, ApJL, 766, L5

Podio, L., Kamp, I., Codella, C., et al. 2014, ApJL, 783, L26

Pontoppidan, K. M., Salyk, C., Bergin, E. A., et al. 2014, Protostars and Planets VI, 363

Pontoppidan, K. M., Salyk, C., Blake, G. A., et al. 2010, ApJ, 720, 887

Porth, O., Fendt, C., Meliani, Z., & Vaidya, B. 2011, ApJ, 737, 42

Prandoni, I., Laing, R. A., Parma, P., et al. 2007, NewAR, 51, 43

Prandoni, I., Laing, R. A., de Ruiter, H. R., & Parma, P. 2010, A&A, 523, A38

Requena-Torres, M. A., et al., 2011, EAS, 52, 299

Qi, C., Öberg, K. I., Wilner, D. J., et al. 2013a, Science, 341, 630

Qi, C., Öberg, K. I., Wilner, D. J., & Rosenfeld, K. A. 2013b, ApJL, 765, L14

Rivilla, V. M. et al. 2015, ApJ, 808, 146

Robert, F., Gautier, D., & Dubrulle, B. 2000, Space Sci Rev, 92, 201

Rosati, P., et al. 2004, AJ, 127, 230

Rygl K. L. J, Brunthaler A., Reid M. J., et al. 2010, A&A, 511, A2

Sakai, N., Sakai, T., Hirota, T., et al. 2014, Nature, 507, 78

Sánchez-Monge Á., Cesaroni R., Beltrán M.T., et al. 2013, A&A, 552, L10

Sánchez-Monge Á., Beltrán M.T., Cesaroni R., et al. 2014, A&A, 569, A11

Sánchez-Monge, Á., López-Sepulcre, A., Cesaroni, R., et al. 2013, A&A, 557, AA94

Sanna A., Moscadelli L., Cesaroni R., et al. 2010, A&A, 517, A78

Sanna A., Cesaroni R., Moscadelli L., et al. 2014, A&A, 565, A34

Santangelo, G., Testi, L., Gregorini, L., et al. 2009, A&A, 501, 495

Santoro, F., et al., 2015, A&A, 574, 89

Schaye, J., Dalla Vecchia, C., Booth, C. M., et al. 2010, MNRAS, 402, 1536

Senatore, F., et al. 2015, A&A, in press

Shapley, A. E. 2011, ARA&A, 49, 525

Simpson, J. M., Swinbank, A. M., Smail, I., et al. 2014, ApJ, 788, 125

Snyder, L. E., Hollis, J. M., Ulich, B. L. 1976, ApJ, 208, L91

Sobolev A. M., Deguchi S., A&A, 291, 569

Swinbank, A. M., Karim, A., Smail, I., et al. 2012, MNRAS, 427, 1066

Tacconi, L. J., Genzel, R., Neri, R., et al. 2010, Nature, 463, 781

Tacconi, L. J., Neri, R., Genzel, R., et al. 2013, ApJ, 768, 74

Taquet, V., López-Sepulcre, A., Ceccarelli, C., Neri, R., Kahane, C., Charnley, S.B., 2015, ApJ, in press

Testi, L., Birnstiel, T., Ricci, L., et al. 2014, Protostars and Planets VI, 339

Thi, W.-F., Ménard, F., Meeus, G., et al. 2011, A&A, 530, L2

Thi, W.-F., van Zadelhoff, G.-J., & van Dishoeck, E. F. 2004, A&A, 425, 955

Tilanus, R. P. J., Krichbaum, T. P., Zensus, J. A., et al. 2014, arXiv:1406.4650

van der Marel, N., van Dishoeck, E. F., Bruderer, S., & van Kempen, T. A. 2014, A&A, 563, A113

van Dishoeck, E. F., Bergin, E. A., Lis, D. C., & Lunine, J. I. 2014, Protostars and Planets VI, 835

Wagg, J., Pope, A., Alberts, S., et al. 2012a, ApJ, 752, 91

Wagner, A. Y., et al. 2012, ApJ, 757, 136

Walsh, C., Millar, T. J., Nomura, H., et al. 2014, A&A, 563, A33

Weber, A. L., 1998, Orig. Life Evol. Biosph, 28, 259

Weiß, A., De Breuck, C., Marrone, D. P., et al. 2013, ApJ, 767, 88

Weiß, A., Walter, F., & Scoville, N. Z. 2005, A&A, 438, 533

Wolk et al. 2005 ApJS 160, 423

Wong, T., & Blitz, L. 2002, ApJ, 569, 157

Woods, P. M., Kelly, G, Viti, S. et al. 2012, ApJ, 750, 19

Woods, P. M. et al. 2013, ApJ, 777, 90

Woon et al. 2002, ApJ, 569, 541

Wu, J., Evans, N. J., II, Gao, Y., et al. 2005, ApJL, 635, L173

Wu, J., Evans, N. J., II, Shirley, Y. L., & Knez, C. 2010, ApJS, 188, 313

Zapata et al., 2004, AJ, 127, 2252

Zinn, P.-C., Middelberg, E., Norris, R. P., & Dettmar, R.-J. 2013, ApJ, 774, 66